Geophysical Journal International

Geophys. J. Int. (2018) **213,** 1701–1719
doi: 10.1093/gji/ggy076
Advance Access publication 2018 February 23
GJI Geomagnetism, rock magnetism and palaeomagnetism

Detrital and early chemical remanent magnetization in redbeds and their rock magnetic signature: Zicapa Formation, southern Mexico

Maria Isabel Sierra-Rojas and Roberto Stanley Molina-Garza

Centro de Geociencias, Universidad Nacional Autónoma de México, Campus Juriquilla, Boulevard Juriquilla 3001*, Querétaro* 76230*, Mexico.*
E-mail: misierra@geociencias.unam.mx

Accepted 2018 February 22. Received 2018 February 6; in original form 2017 June 5

SUMMARY

Poles from continental redbeds are a large fraction of the world's palaeomagnetic database. Nonetheless, the time of acquisition and origin of the remanent magnetization of redbeds has been long debated. We report palaeomagnetic data, rock magnetic data and microscope observations for Lower Cretaceous redbeds in southern Mexico. These data allow us to discriminate between the hysteresis properties of remanent magnetizations of detrital and chemical origin, and to establish the early origin of a chemical remanence. Red sandstones of the Zicapa Formation contain a multicomponent remanence revealed by thermal demagnetization, and consisting of three stable components with partially overlapping laboratory unblocking temperatures of $<250\ ^{\circ}$C, $\sim$300 to $\sim$500 °C and $>600\ ^{\circ}$C, (low, intermediate and high temperature, respectively). They are interpreted as a viscous remanence residing in detrital magnetite, a chemical remanence residing in authigenic hematite and a depositional remanence residing in detrital hematite, respectively. The low-temperature component is nearly parallel to the recent dipole field. The tilt-corrected overall site means of the intermediate (chemical) and high temperature (depositional) components are indistinguishable (Dec = 282.0°, Inc = 12.4°, $k = 13.33$, $\alpha95 = 10.1^{\circ}$, $N = 17$, for the intermediate temperature; and Dec = 272.5°, Inc = 16.5°, $k = 14.04$, $\alpha95 = 11$, $N = 14$, for the high temperature). Elongation/inclination analysis suggests that depositional and chemical components require applying an $f =$ factor of approximately 0.4. Both of these components define a magnetic polarity zonation, but the polarity of the chemical and detrital components may or may not be the same. The chemical remanence coincides, more often than not, with the polarity of the depositional remanence of the overlying (younger) strata, suggesting a delay in remanence acquisition of tens to a few hundred ka for the chemical component. Pigmentary and detrital haematite were recognized with microscopic observations. The particle size of haematite ranges from approximately 10 to 300 μm for detrital haematite (martite, specularite and laterite), and from *ca.* 0.2 to 1 μm for pigmentary haematite flakes. The IRM of these rocks can be modelled with components of low coercivity ($H_{1/2}$ between 5 and 10 mT interpreted as detrital magnetite), and components of a wide coercivity range (prevailing $H_{1/2}$ from $\sim$400 to 600 mT interpreted as haematite). Hysteresis ratios show a systematic correlation with demagnetization behaviour, with lower Hcr/Hc values and higher Mrs/Ms values for samples with a dominant chemical component, than form samples with a significant ($>$40 per cent) depositional component.

Key words: Magnetic mineralogy and petrology; Magnetostratigraphy; Palaeomagnetism; Rock and mineral magnetism.

INTRODUCTION

In the case of redbeds (haematite cemented siliciclastic rocks), controversy exists as to the origin and timing of acquisition of its remanent magnetization. Some authors consider that the natural remanence in redbeds corresponds to a chemical remanent magnetization (CRM) acquired by long-lasting diagenetic processes (Roy & Park 1972; Larson & Walker 1975; Walker *et al*. 1981; Larson *et al*. 1982; Molina-Garza *et al*. 2003). Other authors suggest that the magnetization is provided by ferromagnetic particles, which are oriented with a small bias to the magnetic field during the deposition creating a detrital remanent magnetization (DRM; Elston & Purucker 1979; Tauxe *et al*. 1980; Steiner 1983; Tauxe & Kent 1984; Maillol & Evans 1993; Garces *et al*. 1996; Kruiver *et al*. 2001;

Kodama & Dekkers 2004). Recognizing the mechanism is important because a DRM may be affected by inclination shallowing, while in principle, a CRM will not. Evidence for a primary magnetization residing in detrital specularite in redbeds is supported by particles with high-temperature exsolution textures, and the observation of inclination shallowing error in thin laminations of tabular grains of specularite (Elston & Purucker 1979). Also, the instability of the magnetization that resides in pigmentary haematite compared to magnetization residing in detrital haematite supports the hypothesis that the redbeds characteristic magnetization (ChRM) may be of primary or detrital origin (Collinson 1974; Tauxe *et al*. 1980; Tauxe & Kent 1984).

There are strong arguments, however, that favour a secondary mechanism of acquisition of magnetization in redbeds (Walker *et al*. 1981). By far the most convincing evidence is found in petrographic observations, where a significant fraction of the iron oxides is authigenic. Textural observations suggest they formed by alteration of primary specularite, magnetite, and other Fe-bearing mineral phases; based on these observations and other palaeomagnetic analyses, it has been proposed that remanence acquisition occurs long after deposition (Walker *et al*. 1981; Larson *et al*. 1982; Whidden *et al*. 1998; Beck *et al*. 2003).

Conglomerate and other field tests, as well as magnetostratigraphy in redbeds (Liebes & Shive 1982; Steiner 1983; Molina-Garza *et al*. 1989, 1991, 2003; Tan *et al*. 2007), have shown that the ChRM of redbeds can be both chemical and depositional in origin. The diagenetic processes responsible for the growth of haematite as an authigenic magnetic mineral, however, may be early and sandstones can be magnetized shortly after deposition. In his summary of the redbed controversy, Butler (1998) suggests that the reliability of the magnetization record in redbeds must be considered in a case-by-case basis evaluating, for instance, the relative contributions to the remanence from pigmentary and specular haematite.

The study of the delay in acquisition of magnetization in sedimentary rocks is of importance for magnetostratigraphy and reversal transition studies, as well as investigation of short geomagnetic field events within longer chrons. The delayed magnetization can be considered in some cases a remagnetization, and it depends on whether an earlier magnetization is being replaced by a new one or whether it is the ChRM of the sediment not corresponding to the stratigraphic age (Van der Voo & Torsvik 2012).

The aim of this study is to present palaeomagnetic and rock magnetic data for a Lower Cretaceous redbeds sequence in southern Mexico, in which the natural remanence is interpreted as a combination of a DRM and an 'early acquired' CRM, both residing in haematite. For that purpose, detailed step-wise thermal demagnetization, as well as rock magnetic experiments, were performed. The results suggest that the relative contributions from DRM and CRM vary within a sandstone bed and between beds. A magnetostratigraphic record also suggests that acquisition of a CRM is delayed by tens to hundreds of ka.

It is known that changes in polarity can be recorded by different magnetic phases with variations in the lock-in depth for pDRM or time of precipitation for CRM, indicating that different magnetic phases located in the same stratigraphic level did not acquire their magnetization simultaneously because they did not form at the same time. In the case of the record across transitions of magnetic polarity, the different phases may record two different polarities in the same specimen. An explanation for the presence of both normal and reverse polarities in one specimen is that a polarity is locked-in prior to the transition, being recorded by an early detrital phase, and this is followed by an early chemical magnetization in an authigenic phase formed after the transition. Here we present such a case, where two polarities are recorded in the same stratigraphic level in redbeds. One magnetization corresponds to a DRM that resides in specular haematite of high unblocking temperature (>600 °C), and the other to a CRM residing in pigmentary haematite of intermediate unblocking temperature (250–500 °C).

GEOLOGIC FRAMEWORK

The lower Cretaceous of southwestern Mexico is characterized by a record of magmatism and sedimentation in a volcanic setting, interpreted as allochthonous island arc (s) (Talavera-Mendoza *et al*. 2007), a para-autochthonous arc system (Cabral-Cano *et al*. 2000, Martini *et al*. 2010), or a continental arc (Sierra-Rojas & Molina-Garza 2014). The Lower Cretaceous Zicapa Formation is characterized by the presence of fine- to coarse-grained siliciclastic rocks interbedded with intervals of limestone and calcareous sandstone, deposited in continental to marine transitional environments. The Zicapa Formation contains a record of contemporaneous intermediate calc-alkaline volcanism (Sierra-Rojas & Molina-Garza 2014).

Sedimentology

The data presented here correspond to the Zicapa Formation near its type locality in San Juan de las Joyas, Guerrero State, Mexico (Fig. 1b). The section studied is on the western flank of a latest Cretaceous antiform with a Palaeozoic schist as the oldest unit (Fig. 1b). Here, the Zicapa Formation overlies Middle Jurassic quartz-rich siliciclastic strata of the Tecocoyunca Group, which together with volcanogenic sediments and basement rocks, are the primary source of its detritus. The Zicapa Formation has been divided among five members (Sierra-Rojas & Molina-Garza 2014), but sampling was concentrated in the middle Ajuatetla Member (Fig. 2).

The Ajuatetla Member overlies shallow marine packstone and grainstone beds of the San Juan de las Joyas Member in a transitional contact, and it is characterized by a coarsening-upward section with fine-grained heterolithic beds with ripple cross-laminations. The lack of erosional contacts suggests a continuous and homogeneous sedimentation rate. The siltstones are red to purple in tabular beds with *Thalassinoides*; some conglomeratic beds at the top of this member show trough cross-beds, and are associated with coarse-grained sandstone. A shallow siliciclastic shelf with foreshore deposits is interpreted as the sedimentary environment for this member (Sierra-Rojas & Molina-Garza 2014).

The sandstones of the Ajuatetla Member are litharenites and lithic arkoses, with abundant clasts of metamorphic polycrystalline quartz, monocrystalline quartz, feldspar, albite, metamorphic and felsitic grains. The age range of the deposition for the Ajuatetla Member is determined by the maximum depositional age of a lithic sandstone near the base of the Zicapa Formation of 149 ± 1 Ma (youngest concordant zircon), and the near-depositional age of the volcaniclastic sandstone in the overlying San Andres Member of 133 ± 3 Ma (Sierra-Rojas & Molina-Garza 2014).

SAMPLING AND METHODS

For this study, we sampled a sequence of coarse to very fine lithic sandstones tinted purple to reddish brown. A sequence 190 m thick was described and sampled in the eastern flank of an anticline with an axial plane oriented N20°E (Fig. 1b) and sampled at a

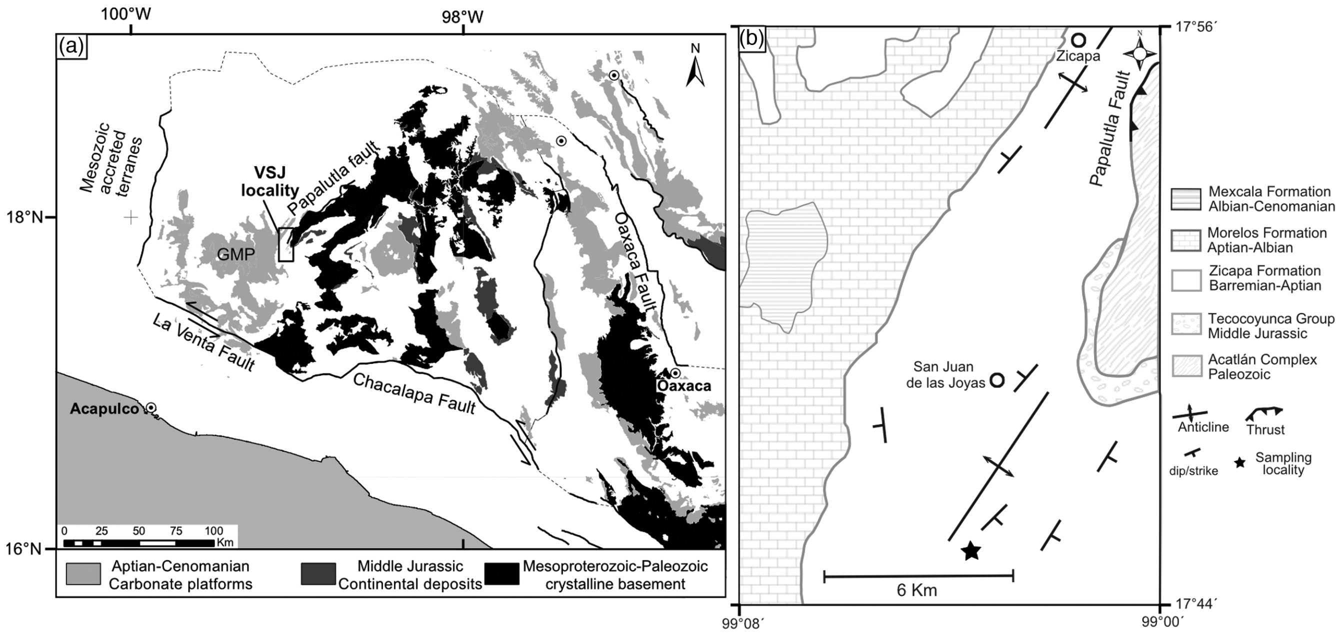

Figure 1. (a) Localization of the San Juan de las Joyas (VSJ) area and sampling sites in a map showing the distribution of Cretaceous strata in southern Mexico. GMP: Guerrero-Morelos platform. (b) Geologic map of the area of the San Juan de las Joyas locality.

total of 19 sites (Fig. 2b). Six to eight samples were drilled with a gasoline portable drill obtaining 2.5 cm diameter cores 6–12 cm deep; the samples were oriented in the field with magnetic and solar compasses, as well as an inclinometer. Each site was collected from a single bed, and site spacing depended on the availability of suitable material in the section. In the laboratory, the cores, 117 in total, were cut into 2 cm long specimens, obtaining two to four specimens for sample. All magnetic measurements were made at the palaeomagnetic laboratory of the Centro de Geociencias, UNAM, at the Juriquilla campus.

The natural remanent magnetization (NRM) was measured using a JR-5 spinner magnetometer housed in a shielded room. A set of samples, one for each site, were subjected to progressive alternating field (AF) pilot demagnetization tests, using an LDA-3A Demagnetizer (AGICO), exposing the samples to inductions from 1 to 100 mT in steps not larger than 10 mT. After the AF pilot test, the samples were subjected to thermal demagnetization in air in a thermal demagnetizer TD-48 SC (ASC-Scientific). The specimens were progressively heated from room temperature to 500 °C every 50 °C and from 500 to 650 °C in 25 °C steps. After every heating step the NRM and magnetic susceptibility were measured for each one of the specimens. For the visualization and analysis of the results of the demagnetization experiments, we used orthogonal demagnetization diagrams (Zijderveld 1967) and equal-area stereographic projections (Figs 3 and 4). The remanence vector directions were determined in each specimen using principal components analysis (Kirschvink 1980), and then the mean for each site was calculated; the site means were calculated assuming the distribution of directions of Fisher statistics. The data-set was further examined to evaluate the fit to a Fisher distribution.

Rock magnetic experiments were used to characterize magnetic carriers (a minimum of one specimen per site). Hysteresis parameters (Ms, Mrs, Hc and Hcr), isothermal remanent magnetization (IRM) and backfield curves of saturation of IRM were determined with a Princeton Measurements Corp. MicroMag 2900 vibrating sample magnetometer. The IRM acquisition curves were modelled by the first derivative method, allowing one to infer the magnetic mineralogy of a sample based on its coercivity spectra (Kruiver *et al.* 2001). Thermomagnetic curves were obtained in a custom-made Curie balance using approximately 3.5 g of pulverized sandstones in a DC field of 0.4 T in air, with heating-cooling rates of 30–40 °C min^{-1}. A Lowrie test was performed applying fields of 3, 0.5 and 0.15 T along three orthogonal directions. Then the samples where thermally demagnetized up to 660 °C in 50 and 20 °C steps. The petrography of samples was studied in thin sections with a petrographic microscope of polarized light (Olympus Bx-51), and textures of magnetic oxides were studied with a scanning electron microscope (SEM).

RESULTS

Palaeomagnetism

AF demagnetization caused a small change in the NRM, except in very few sites, leading one to conclude that most of the magnetization resides in phases of high coercivity such as haematite. In 80 per cent of sites, AF demagnetization resulted in the removal of a north-directed remanence. Thermal demagnetization revealed that the remanent magnetization in the rocks of the Zicapa Formation is relatively complex, with a multivectorial behaviour. Some of the rocks show two-components (Figs 3a and b); the component removed at low temperatures is designated as low-temperature component (LTC). It has a north to northwest-directed declination and is of moderate positive inclination. This component is generally completely removed after heating to 200 °C. An abrupt decay upon heating to 100 °C was observed at two sites (Fig. 3b) where this component is prominent. A univectorial decay is observed after removing the LTC, showing distributed laboratory unblocking temperatures between 250 °C and >650 °C (Fig. 3); most of the specimens show a linear trend to the origin. The magnetization component defined in this interval of demagnetization is northwest to west-northwest directed with moderate positive inclination, or its antipode of negative inclination and southeast declination (Figs 3d and e; VSJ9A2, VSJ13B). Upon further examination of the unblocking temperatures is evident that in some cases

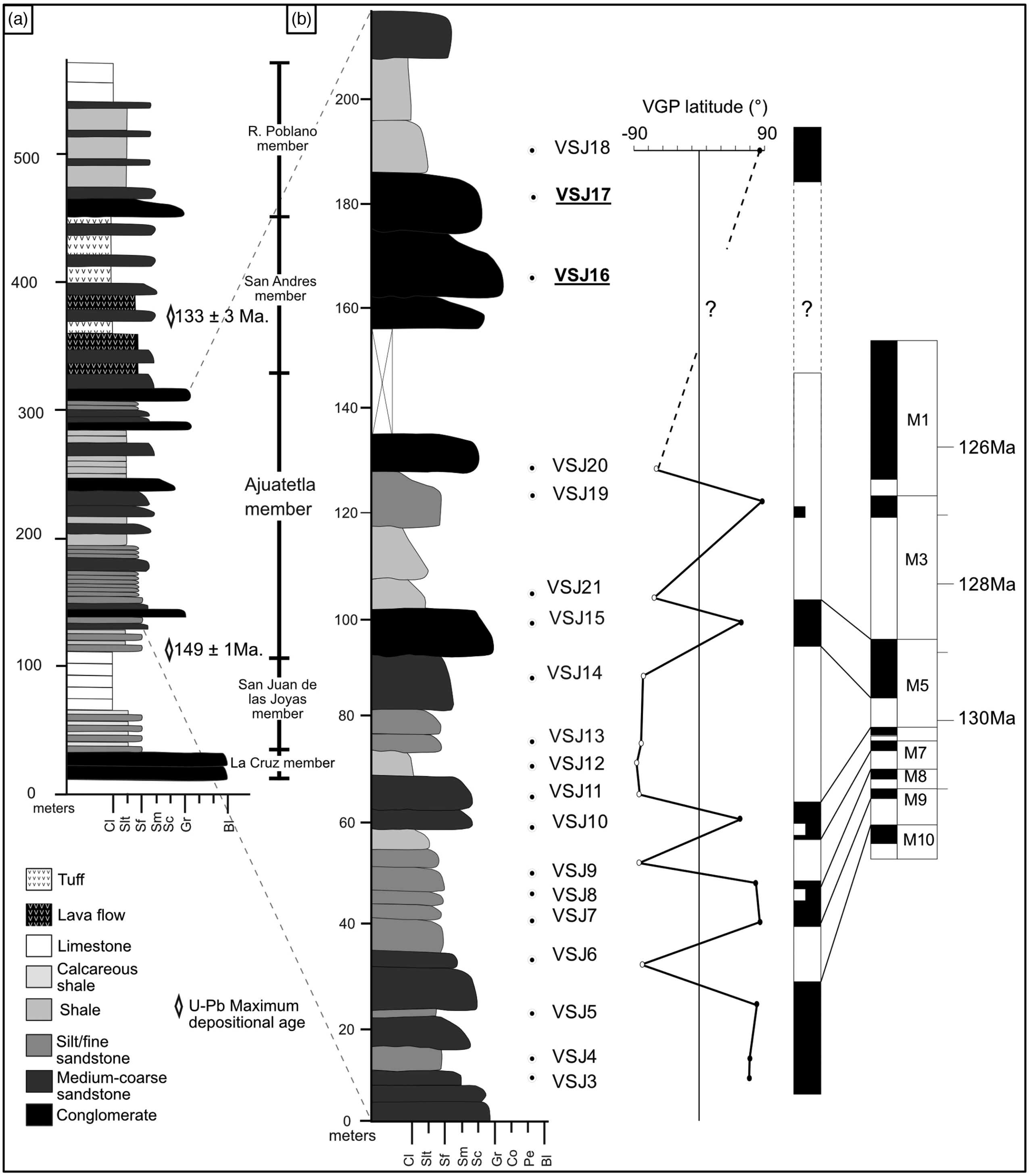

Figure 2. (a) A generalized column of the Zicapa Formation. (b) Stratigraphic section and magnetostratigraphy of the Ajuatetla Member, Zicapa Formation (base: 17.77457, −99.0813; top: 17.76489, −99.08405). The location of the sampling sites is shown in each stratigraphic level. We also include a plot of virtual geomagnetic pole (VGP) latitude versus stratigraphic level. The black bars represent normal polarity intervals and the white bars reverse polarity intervals. The magnetic polarity zonation is correlated with the geomagnetic scale for the Early Cretaceous (Ogg 2012).

the remanence decays primarily between approximately 300 and 600 °C (Fig. 3b), while others show greater decay at higher temperatures above 600 °C (Figs 3d and e).

Some of the samples show more complex magnetization records, wherein at least three magnetizations components contribute to the NRM (Fig. 4). An LTC is again north to north-west directed and of moderate positive inclination, of obout 40 °C; again, this is removed by heating to 200 °C. A second component is of intermediate laboratory unblocking temperature (intermediate-temperature component, ITC), and is defined between 250 °C and approximately 500 °C; this component is northwest directed and moderate positive inclination, or its antipode. The high-temperature component

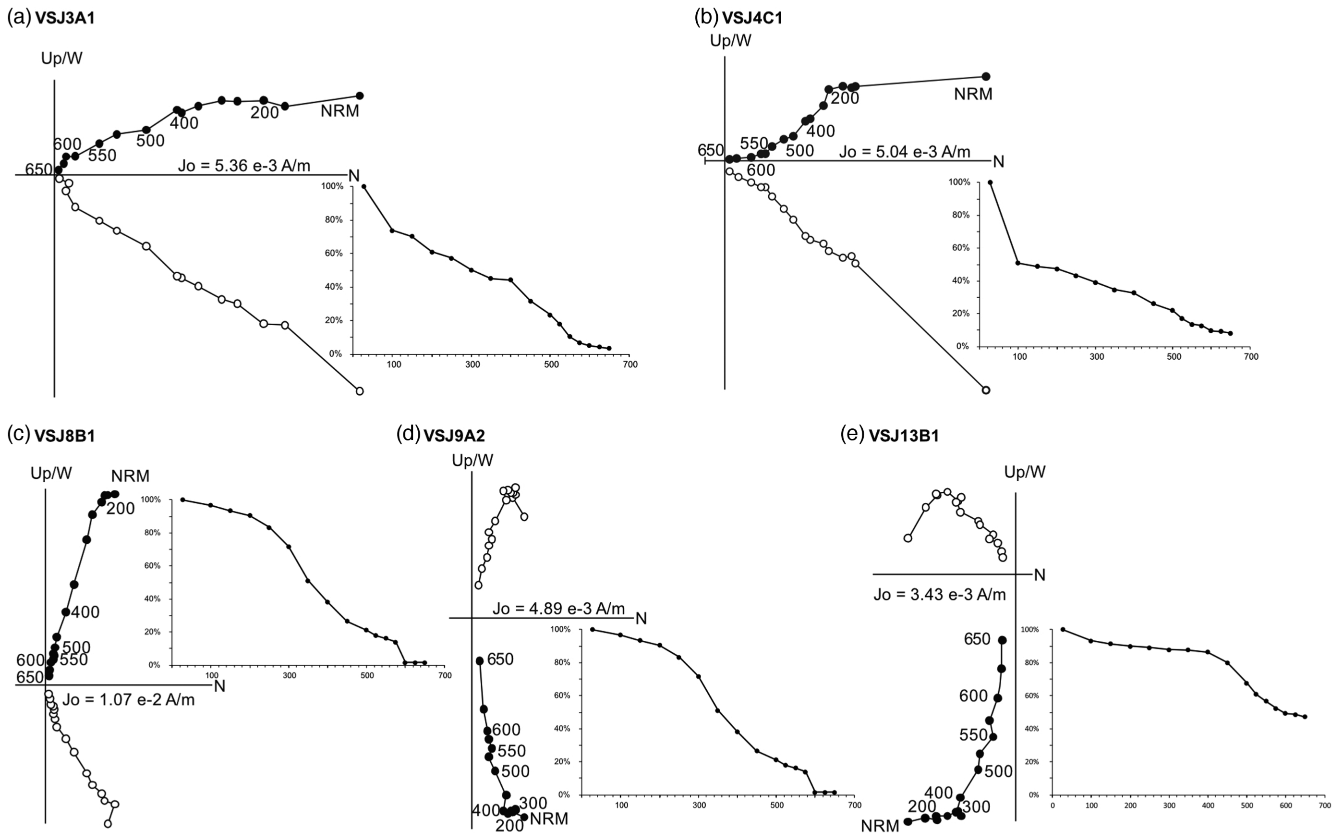

Figure 3. (a–e) Representative examples of orthogonal demagnetization diagrams and evolution of the remanence intensity (normalized with respect to the maximum J0) during thermal demagnetization. The samples show apparent univectorial or two NRM components. The characteristic magnetization, defined in the range 250 to over 650 °C, is overprinted by a small secondary component, which is mostly north-directed and of positive inclination (a and b). Closed (open) circles correspond to the projection of the NRM vector onto the horizontal (vertical) plane.

(HTC) is defined in temperatures over 600 °C, and it is west to west-northwest directed with a positive moderate inclination (or its antipode). Thus two near parallel components were recorded in some specimens, and two antipodal components were recorded in others. Occasionally the demagnetization diagrams show curved trajectories (Fig. 4c), suggesting that unblocking temperature spectra of the three components overlap to some degree.

Mixed polarities are observed within a single site for the ITC, such as at VSJ5, VSJ6, VSJ12, VSJ13, VSJ19 and VSJ20; HTCs, in contrast, are of uniform polarity within a site. When samples are analysed in a stratigraphic context, important details are observed, as follows. If adjacent sites are of opposite polarity, the ITC more often than not corresponds to the direction of the HTC of the overlying site. This behaviour is observed, for instance, at siteVSJ6 where the ITC is of mixed but predominantly normal polarity, HTC is of reverse polarity, while HTC is normal at the overlying site VSJ7. Similarly, the polarity of the HTC of VSJ14 is of reverse polarity, while the ITC is a normal polarity corresponding to the polarity of the HTC of overlying site VSJ15 (Fig. 5). Yet another example is VSJ19, where the ITC is of mixed but mostly reverse polarity, the HTC is of normal polarity, and the ITC corresponds to the reversed polarity of the HTC of VSJ20 above. After these observations were made, we calculated the directions of vectors corresponding to unblocking temperatures of the ITC and the HTC at each stratigraphic level. We made this calculation even if the components appear colinear (as in Fig. 3). When mixed polarities occur in the ITC we inverted directions to the dominant polarity in the site to report a single polarity. Results of these calculations are in Tables 1 and 2.

The polarity zonation in all the Ahuejutla Member sites was determined from end-point directions for the HTC, and occasionally demagnetization trajectories. For the mean direction, four sites were excluded due to large within-site dispersion, an insufficient number of samples, or an unstable behaviour during demagnetization. Nine magnetic polarity zones were recognized in the locality (Fig. 2b).

Overall means were calculated using Fisher's statistics (Fisher 1953) inverting reverse polarity magnetizations. The low-temperature component of magnetization in all sites is close to the present-day field direction at the sampling location, so it is interpreted as viscous remanent magnetization and will not be further discussed. The ITC and HTC of magnetization form two indistinguishable populations, both with bipolar distributions (Tables 1 and 2). The ITC and the HTC group means are, *in situ*, west-directed and of moderate positive inclination (Fig. 6) that become moderately shallow after tilt correction. The tilt corrected means of the ITC and HTC components are: Dec = 282°, Inc = 12.4° ($k = 13.33$, $\alpha95 = 10.1°$, $N = 17$) and Dec = 272.5°, Inc = 16.5° ($k = 14.04$, $\alpha95 = 11$, $N = 16$), respectively. In tilt corrected coordinates both groups pass the reversal test of McFadden & McElhinny (1990) with a positive reversal test classification or 'Rb' (Tables 1 and 2). The ITC and HTC means are statistically indistinguishable.

Elongation–inclination correction

A flattened directional distribution of sample directions suggests the possibility of an effect of sedimentary shallowing of the inclination. We performed an elongation–inclination (*E*/*I*) correction in

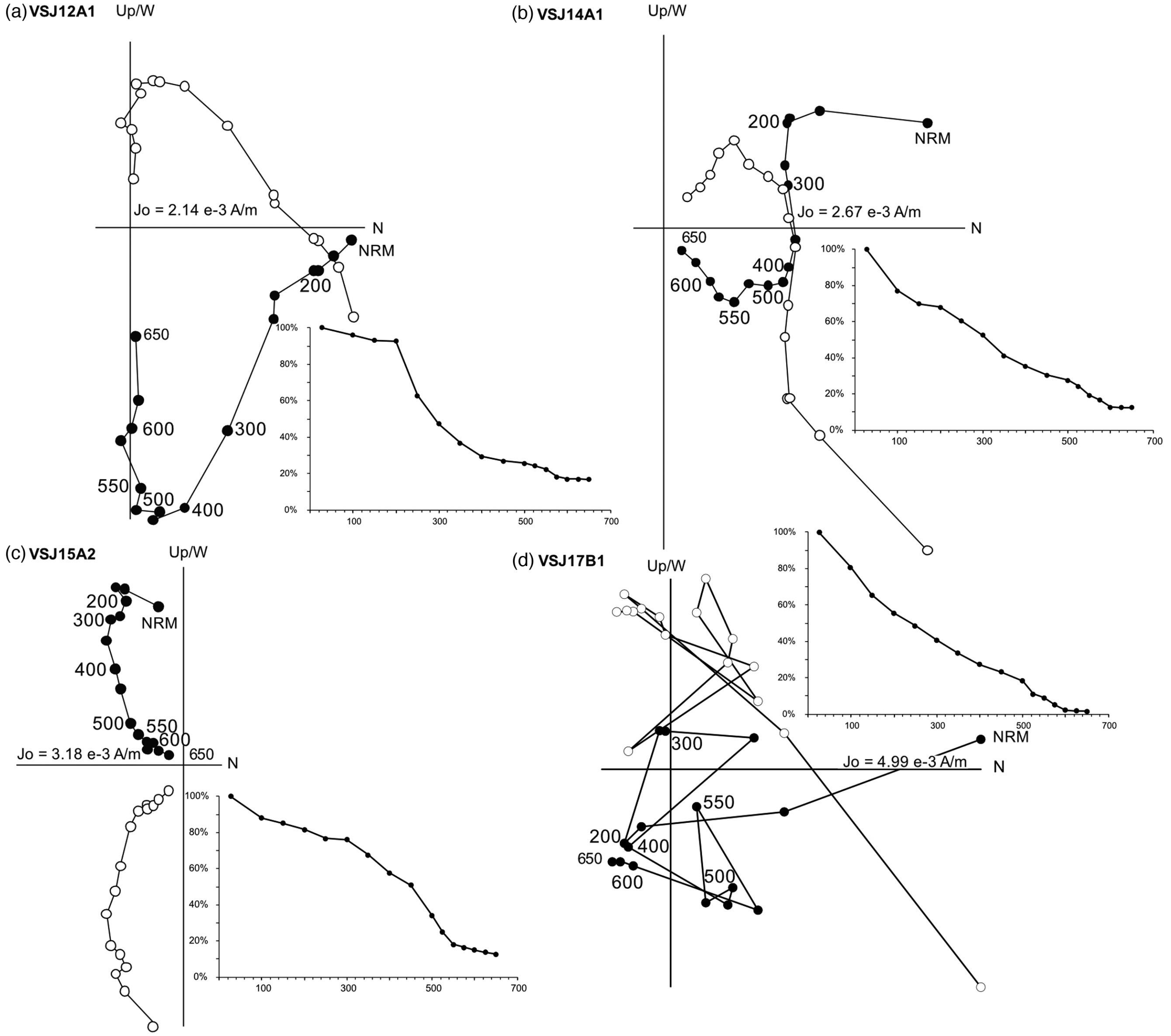

Figure 4. Examples of orthogonal demagnetization diagrams and evolution of the remanence intensity (normalized with respect to the maximum J0) during thermal demagnetization for samples with multivectorial behaviour. (a–c) Samples with three components showing a near present-day field magnetization (NRM-200 °C), an intermediate laboratory unblocking temperature magnetization (250–400 °C), and a high-temperature magnetization component (>575 °C). (d) VSJ17B shows a well-defined low unblocking temperature component and an erratic behaviour after 250 °C. Symbols as in Fig 3.

both ITC and HTC to evaluate the effect of inclination shallowing (Tauxe & Kent 2004). For the analysis, we used 114 sample directions for the ITC and 110 for the HTC (Figs 7a and d). The *E*/*I* technique can give inaccurate results if there are vertical axis rotations between sites, but these rotations are considered unlikely because a continuous section of near uniformly dipping strata was sampled. For the ITC the original distribution of samples directions shows a mean principal eigenvector of $D = 283.1^\circ$, $I = 13.5^\circ$ with an initial eccentricity of $E = 1.816$ and an elongation to the NW or SW. The *E*/*I* analysis determined a crossing-point model for the data (Figs 7b and c) predicting inclination of $I = 28^\circ$, which represents the inclination versus elongation pair more consistent with the geomagnetic model; this indicates a flattening factor of $f = 0.41 + 0.34/-0.49$ and an eccentricity of $E = 2.3272$. The HTC original distribution is also elongated to the NW and SW and shows mean eigenvector direction of $D = 277.8^\circ$, $I = 14.7^\circ$ and an initial eccentricity of $E = 1.617$. The model predicts an inclination $I = 34.6^\circ$ (Figs 7e and f), eccentricity $E = 2.1412$, and a flattening factor $f = 0.4 + 0.32/-0.55$. In both cases there is a greater dispersion in declination than inclination, as observed when flattening is suspected. The overall means of the ITC and HTC sample directions after correcting for inclination shallowing with an *f*-factor of 0.4 are $D = 282.0$, $I = 28.2^\circ$, and $D = 272.5$, $I = 36.5^\circ$, respectively.

When the overall means are compared with the expected direction, assuming stability with respect to the North America craton and using the reference pole of Torsvik *et al*. (2012), they are discordant; the discordance is primarily in declination. Using the directional-space approach to analyse the vertical-axis rotations and the latitudinal motions from palaeomagnetic directions (Beck 1980; Demarest 1983), the ITC indicates R and F (rotation and flattening

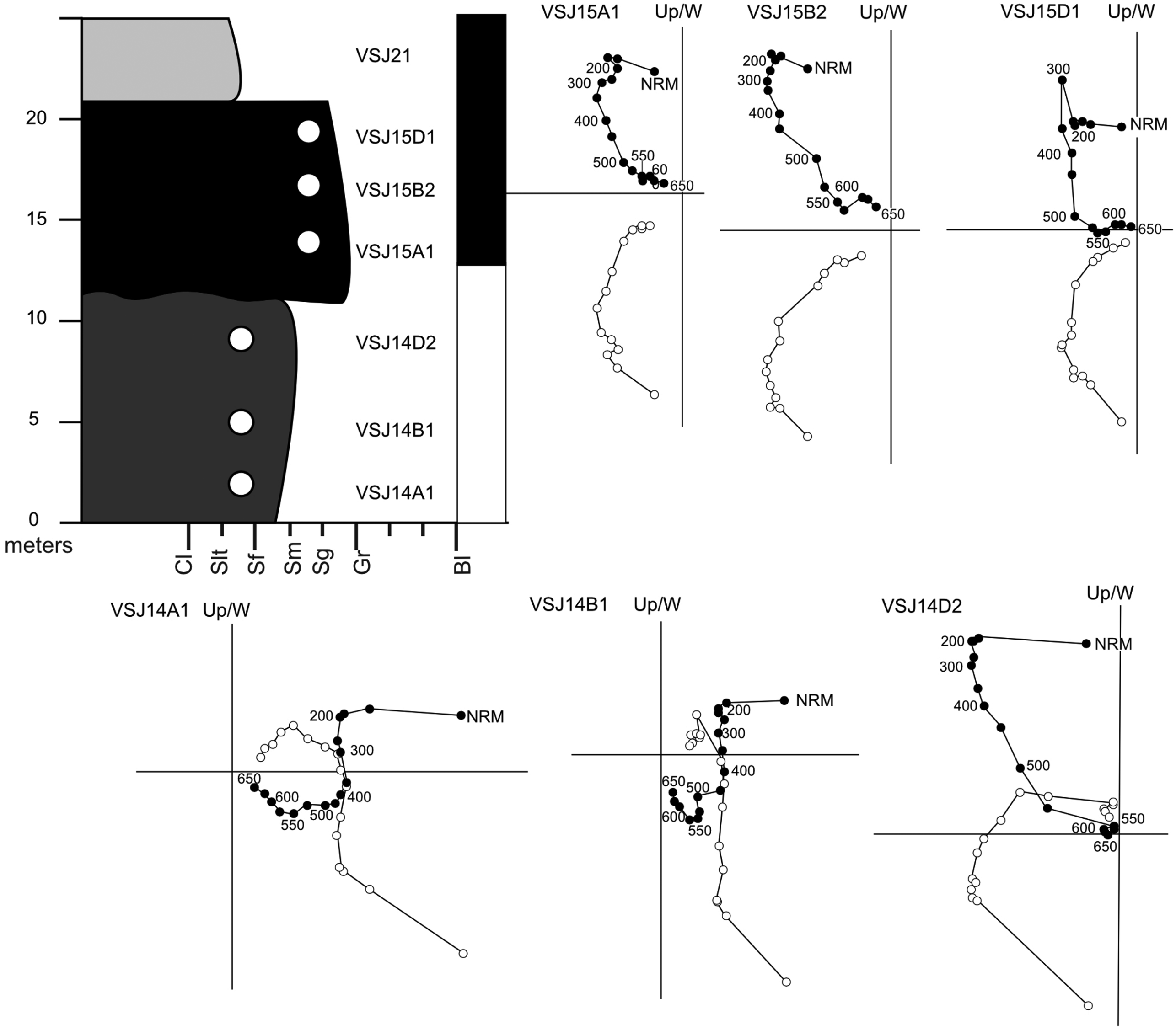

Figure 5. Interval with polarity transition from reverse to normal of the high-temperature component. In the lower site (VSJ14) the HTC (DRM) is reverse in all three samples and the ITC (CRM) is normal, as the HTC of the overlying site.

parameters) of -58.6 ± 10.1 and -16.8 ± 12.7. The HTC indicates values of R and F of -69.2 ± 10.1 and -7.7 ± 13.0. The F value for HTC is not discordant in inclination.

Rock magnetism

The results of AF and thermal demagnetization experiments suggest that the remanence resides in one or more magnetic phases. For instance, resistance to AF demagnetization and the observation of components that reside in intermediate (250–500 °C) and high maximum unblocking temperatures (600–650 °C) suggest that there are varying contributions to the remanence from possibly fine-grained authigenic and coarser detrital haematite (Collinson 1974). This hypothesis is further explored in rock magnetic experiments.

Representative thermomagnetic curves for samples of pulverized sandstones are shown in Fig. 8. The cooling cycle shows that there are mineralogical changes caused by laboratory heating of the samples, possibly oxidation because the curves are not reversible and decrease their magnetic moment upon cooling. In the heating cycle, the inflection at ~580 °C confirms the presence of magnetite in some samples. All the samples are characterized by a change in the slope above 620 °C associated with the Neel/Curie temperature of haematite with a small degree of cation substitution (assumed to be both pigmentary and detrital hematite). In the sample of Fig. 8(b) the intensity of magnetization increases upon cooling, but very slightly. There are no signs of maghemite inversion, we, therefore, conclude that magnetite and haematite are present in varying proportions, but magnetite may be absent (e.g. VSJ3). Again, considering the low saturation magnetization of haematite compared to magnetite, it is evident that, when present, by volume magnetite occurs in significantly smaller proportion.

Examples of hysteresis acquisition curves are shown in Fig. 9. The loops show a variety of shapes, but almost all of them are constricted in the middle section of the loop and widen in the lower and upper sections; this morphology has been defined as a 'wasp-waisted' hysteresis loop (Roberts *et al*. 1995; Tauxe 1996). We distinguish three types of curves in terms of the geometry of the

Table 1. Palaeomagnetic data for intermediate-temperature component (ITC) obtained from 350 to 600 °C. Inclination before *E*/*I* correction.

		In situ					Tilt corrected				
Samples	*n*/*N*	Dec(°)	Inc(°)	*k*	α_{95}	Dip/Strike	Dec(°)	Inc(°)			
VSJ18	7/7	275.8	27.4	79.2	6.8	175, 5	275.6	22.4			
VSJ17*	2/2	102.2	−21.6	–	–	156, 17	109	66.2			
VSJ20	3/10	58.6	−52.8	25.9	24.7	145, 16	59.2	−37.8			
VSJ19	6/8	87	−30	39.6	10.8	145, 15	84.3	−16.4			
VSJ21	3/3	289.8	21.2	38.4	2.9	85, 20	281.2	26.3			
VSJ15	3/3	253.4	40.1	58.1	16.3	221, 30	267.3	20.7			
VSJ14	4/6	263.2	44.8	83.5	10.1	221, 30	276.5	21.8			
VSJ13	3/4	110.1	−28.6	39.8	19.8	221, 30	112.7	−0.3			
VSJ12	11/11	101.2	−32.3	13.9	12.7	221, 30	106	−5.5			
VSJ11	6/8	86.2	−26.4	15.7	17.4	221, 30	91.8	−3.9			
VSJ10	5/5	298	15.4	42.4	11.9	191, 30	297.8	−13.4			
VSJ9	8/9	92.5	−33.5	42.1	8.6	191, 30	93.9	−3.8			
VSJ8	8/8	289.7	26.7	75.3	6.4	191, 30	288.8	−3			
VSJ7	4/4	287.3	27.4	400.1	4.6	191, 30	286.6	−2.4			
VSJ6	6/9	119.8	−42.4	26	13.4	231, 15	123.4	−28.2			
VSJ5	4/4	257.2	39.1	7.3	36.4	201, 30	264.7	12.9			
VSJ4	9/9	295	29.2	49.6	7.4	201, 30	294.5	−0.7			
VSJ3	6/8	336.1	44.9	47.3	9.8	201, 30	323.6	21.2	**k**	**α_{95}**	**n**
Mean normal	10	284.5	33.5	14.46	13.1		285.5	11.1	14.09	13.3	10
Mean reverse	7	94.8	−36.3	21.84	13.2		96.8	−14.3	11.69	18.4	7
Overall mean	**17**	**276.9**	**37.3**	**8.38**	**13.1**		**282**	**12.4**	**13.33**	**10.1**	**17**

Table 2. Palaeomagnetic data for high-temperature component (HTC) obtained from 600–650 °C. Inclination before E/I correction.

			In situ					Tilt corrected			
Samples	n/N	Dec(°)	Inc(°)	k	α_{95}	Dip/Strike	Dec(°)	Inc(°)			
VSJ18	4/6	278.6	28.5	95.4	9.5	175,5	278.3	23.5			
VSJ20	8/10	65.5	−50.2	56	7.5	145,16	64.5	−35.2			
VSJ19	4/6	276.1	29.6	7.8	35.2	145,15	272.5	17			
VSJ21	3/4	83.3	−41.1	6.9	46	85,20	67.8	−35.7			
VSJ15	3/3	209.7	48.9	17.9	30	221,30	243.4	45.8			
VSJ14	3/5	65.6	−39.5	11.1	5.8	221,30	81.4	−23			
VSJ13	5/5	94.8	−21.1	25.3	15.5	221,30	97.5	3.7			
VSJ12	9/9	88.4	−32.7	147.9	4.2	221,30	95.8	−9.1			
VSJ11	4/8	89.6	−21.3	166	7.2	221,30	92.9	2			
VSJ10	2/3	129.5	−26.7	–	–	191,30	126.2	0.2			
VSJ9	8/8	95.6	−31.8	62.6	7.1	191,30	96.4	−1.9			
VSJ8	7/7	281.1	37.3	15.4	17.6	191,30	281.1	7.4			
VSJ7	4/4	274.6	42.5	28.8	17	191,30	276.2	12.6			
VSJ6	8/9	98.2	−30.2	21.3	12.6	231,15	102.7	−18.8			
VSJ5*	1/5	256	37	–	–	201,30	263.2	11.2			
VSJ3*	2/8	294	48	–	–	201,30	293.1	18	**k**	**α_{95}**	**n**
Mean normal	5	267.8	40	12.22	22.8		272	21.6	17.18	19	5
Mean reverse	9	91.2	−34	19.82	11.9		92.8	−13.6	12.06	15.5	9
Overall mean	**14**	**90.1**	**−36.1**	**17.3**	**9.8**		**92.5**	**−16.5**	**14.04**	**11**	**14**

loops as well as hysteresis parameters (Özdemir & Dunlop 2014). The first type is represented by only one sample, VSJ17 (Fig. 9c), with low bulk coercive force, Hc (0.013 T), low remanent coercive force, Hcr (0.0039 T), and an incipient ‘wasp-waisted’ loop. This sample is near saturation at inductions of approximately 1 T, thus the low coercivity is not solely caused by a cubic phase such as magnetite; magnetite is, however, evidently present. Sample VSJ17 shows a rather steep IRM acquisition curve with up to 70 per cent of the remanence acquired below 0.1 T, but the sample does not reach saturation until it is exposed to inductions of approximately 1 T (see the discussion of IRM below). Therefore, the low coercivity observed in the hysteresis loop does not indicate the presence of a single cubic phase such as magnetite of varying grain-sizes; the hysteresis loop suggests that magnetite overwhelms the signal from hematite. The second and more common curve type is the typical ‘wasp-waisted’ hysteresis loops, with coercive force values ranging from 0.105 to 0.319 T, and ratios of remanent saturation to saturation magnetization (Mrs/Ms) of up to 0.53 (Figs 9d–f). The third curve type corresponds to the ‘goose-neck’ hysteresis loops (VSJ4, Fig. 9a) with the high Hc value (0.3 T). Type 2 and 3 curves are far from saturation even at inductions of 2 T; these curves also show high Mrs/Ms values between 0.27 to 0.58 and Hcr/Hc ratios of approximately 1.5 to 3.5 (Fig. 10), which are consistent with SD haematite behaviour (Özdemir & Dunlop 2014).

As we considered the ChRM to reside primarily in hard magnetic phases with different grain-size (and inherently different coercivity), a components analysis of the IRM is necessary to properly identify and quantify the contributions from different magnetic carriers. We modelled the IRM acquisition curves (Kruiver *et al*. 2001) for the sandstones of the Zicapa Formation. In all samples, IRM

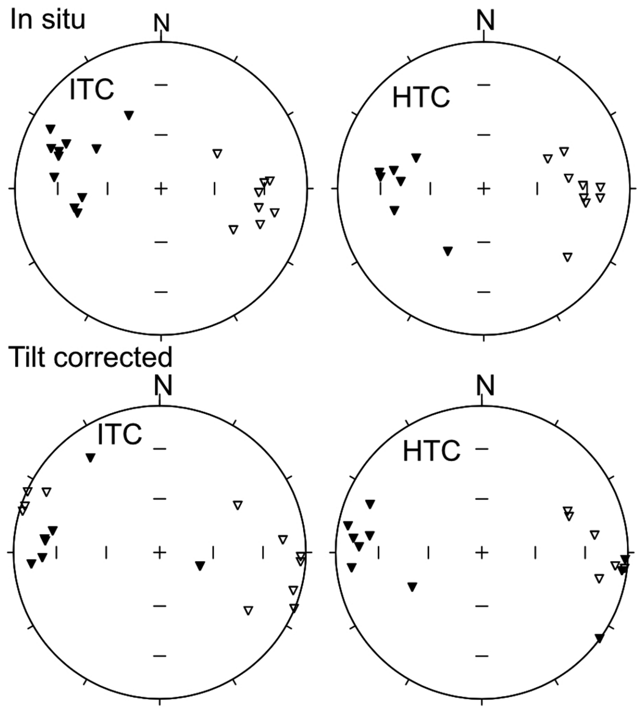

Figure 6. Site means *in situ* (above) and tilt corrected (below) directions isolated components of the VSJ locality. Left: site means of the intermediate-temperature component (ITC). Right: site means for the characteristic remanent magnetization (ChRM) of the high-temperature component (HTC). Close triangles for normal polarity and open triangles for reverse polarities.

acquisition curves were modelled with more than one component (Fig. 11). Generally, the dominant mineral phase shows high coercivities (H1/2 = ∼500–600 mT), this phase makes generally ∼85 to 90 per cent of the total IRM. In the sample from site VSJ4 (Fig. 11d), the dominant coercivity phase exceeds 800 mT, in agreement with very high Hc values observed in hysteresis experiments.

A very low coercivity phase (<10 mT) is necessary to model some of the curves (Fig 11a). This component may contribute to the IRM as much as 10 per cent, and it most likely contributes to the NRM because it is associated with sites where a large north-directed and positive inclination component was observed. A very small component (<5 per cent of the IRM) with maximum coercivities of approximately 1 and 1.5 T was used to fit the IRM curve in some samples (Figs 11a and c). Finally, a moderately high coercivity component was required to fit most of the curves; it makes generally approximately 10 per cent of the IRM and has a mean coercivity of *ca.* 30–100 mT. This component is present in small proportion at nearly all sites. The low coercivity values of about 30 are consistent with a magnetite-like phase, but coercivities above 50 mT are too high to indicate that they are solely in magnetite (e.g. Dunlop 1986; Sagnotti *et al*. 2006), even uniaxial single-domain magnetite, and it is probably associated with some forms of very fine pigmentary haematite or perhaps maghemite.

The samples modelled with a dominant contribution of the high coercivities (i.e. >400 mT; Fig. 11) are consistent with the results from the thermomagnetic curves and the hysteresis loops, indicating the predominance of haematite. Sample VSJ17 is interesting in that the coercivity values used to model the curve are significantly lower than at other sites (Fig 11a). The high coercivity component of

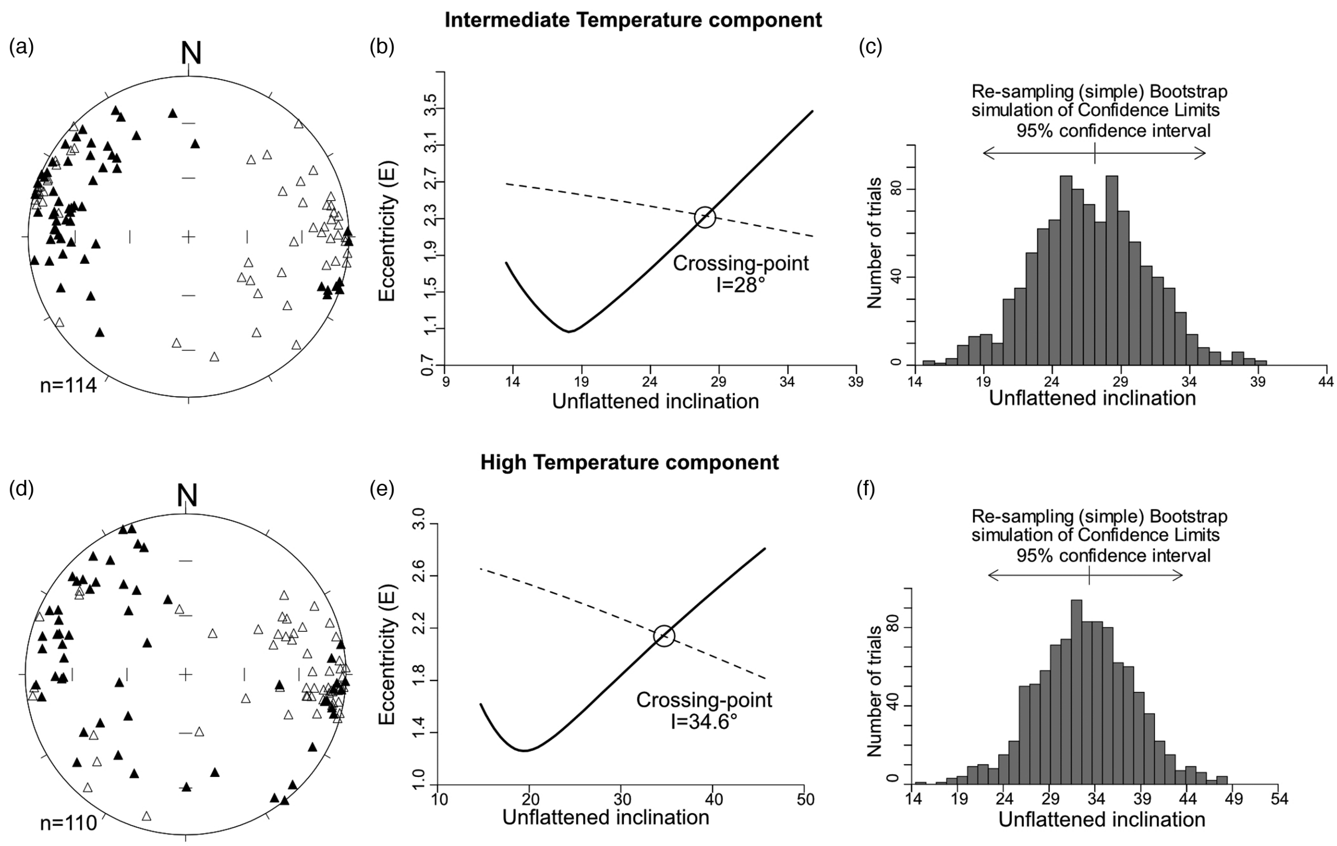

Figure 7. Elongation–inclination correction (Tauxe & Kent 2004) performed at all sites with lithologies that vary from fine-grained to coarse-grained clean sandstones. (a and d). Equal-area projections of the sample directions for the ITC and HTC, respectively. (b and e) Plots of elongation versus inclination of the data in (a) and (d), respectively. (c and f) Histogram of crossing point from 1000 bootstrap simulations of confidence limits.

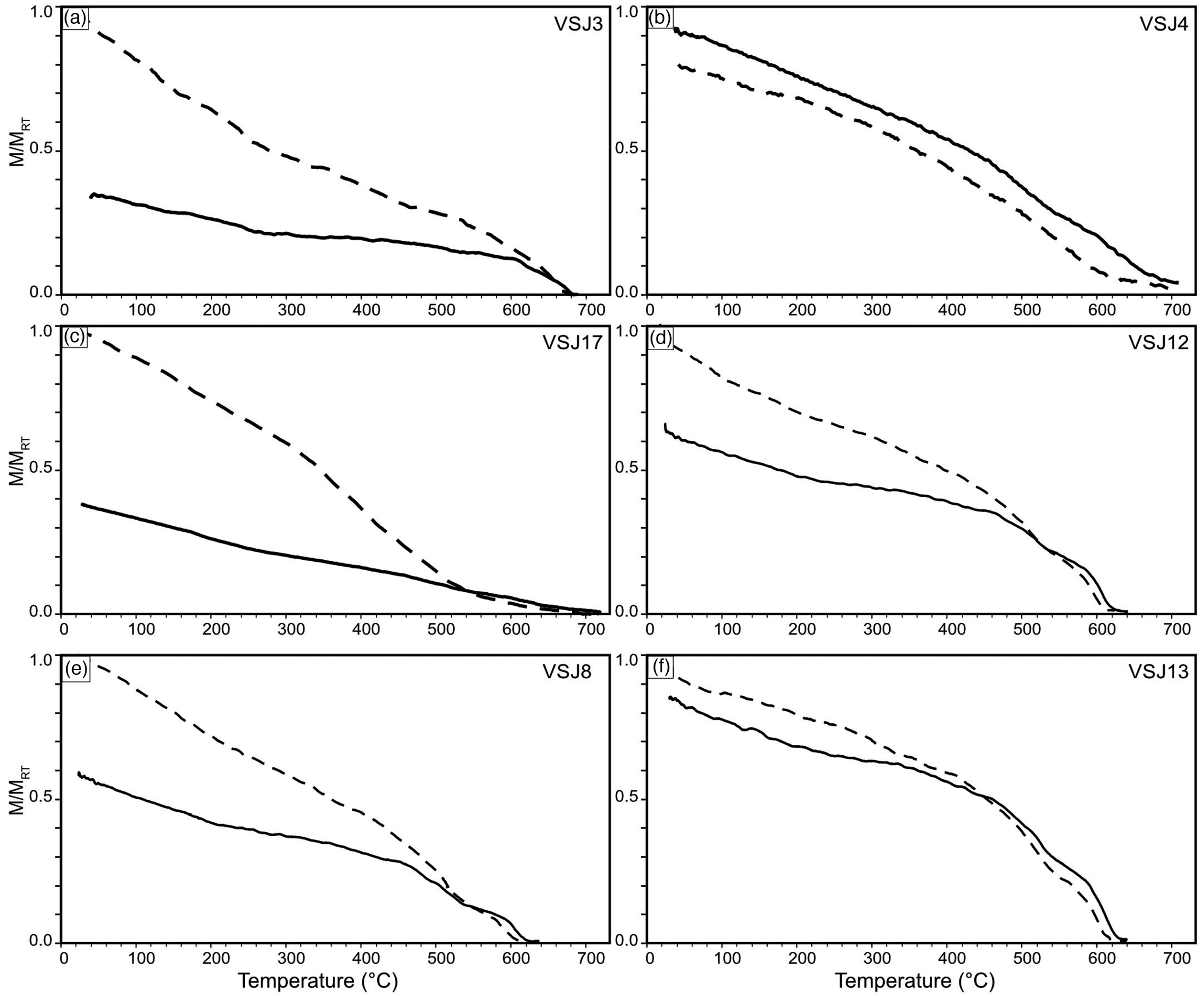

Figure 8. Representative thermomagnetic curves showing the heating cycle in dotted line and the cooling cycle in solid line. All the samples are heated in air from room temperature up to 700 °C. Samples VSJ3, VSJ4 with haematite (a,b), VSJ17, VSJ12, VSJ8, VSJ13 with both magnetite and haematite (c–f).

approximately 500 mT is not required to model the VSJ17 IRM acquisition curve, we used instead of a component with H1/2 = 200 mT. Also, the hysteresis loop is narrower than for other sites (Fig. 9c); despite having a loop associated with a mixture between different coercivities or grain sizes, it presents the lowest Hc and the narrowest loop, and haematite is barely visible in the thermomagnetic curve (Fig. 8c). This sample is also associated with unstable demagnetization behaviour (Fig. 4d), and we failed to isolate a HTC at this site.

Lowrie test

The rock magnetic experiments previously described indicate the presence of a mixture of low and high coercivity magnetic minerals, and suggest the presence of goethite in some samples. In order to better understand the remanence carriers, we performed a Lowrie test to evaluate the presence of goethite, haematite, and magnetite (Lowrie 1990). A subset of nine samples was used to perform the test, applying inductions of 3, 0.5, and 0.150 T in three orthogonal directions using a pulse magnetizer. The specimens were subsequently demagnetized up to 660 °C in 50–20 °C steps. Thermal demagnetization of IRM components reveals that the dominant magnetic phases are of coercivity greater than 150 mT, making (combined) 85 to 98 per cent of the remanence (Fig. 12). In all the samples the IRM components induced at 0.5 and 3 T have distributed laboratory unblocking temperatures between about 200 and 600 °C and a maximum unblocking temperature near 660 °C (Fig. 12). Both the hard and intermediate components (3 and 0.5 T respectively) thus reside in haematite. We observed a hint of goethite in one of the samples analysed (VSJ6, Fig. 12d), with a small decrease of about 15 per cent in the hard IRM component. Goethite is however absent in the other samples analysed. Magnetite is present in most samples but in low concentration. We observed decay of the soft IRM component (<150 mT) at temperatures near 580 °C (it was observed in five of the samples used for the test, Samples VSJ5, and VSJ8, Fig. 12), but clear inflections in the decay curve are not observed in the 550–590 °C range; furthermore, as little as 5 per cent or as much as 30 per cent of the soft component unblocks at temperatures of about 650 °C, and thus resides in haematite. In sample VSJ12 the soft component is less than about 2 per cent of

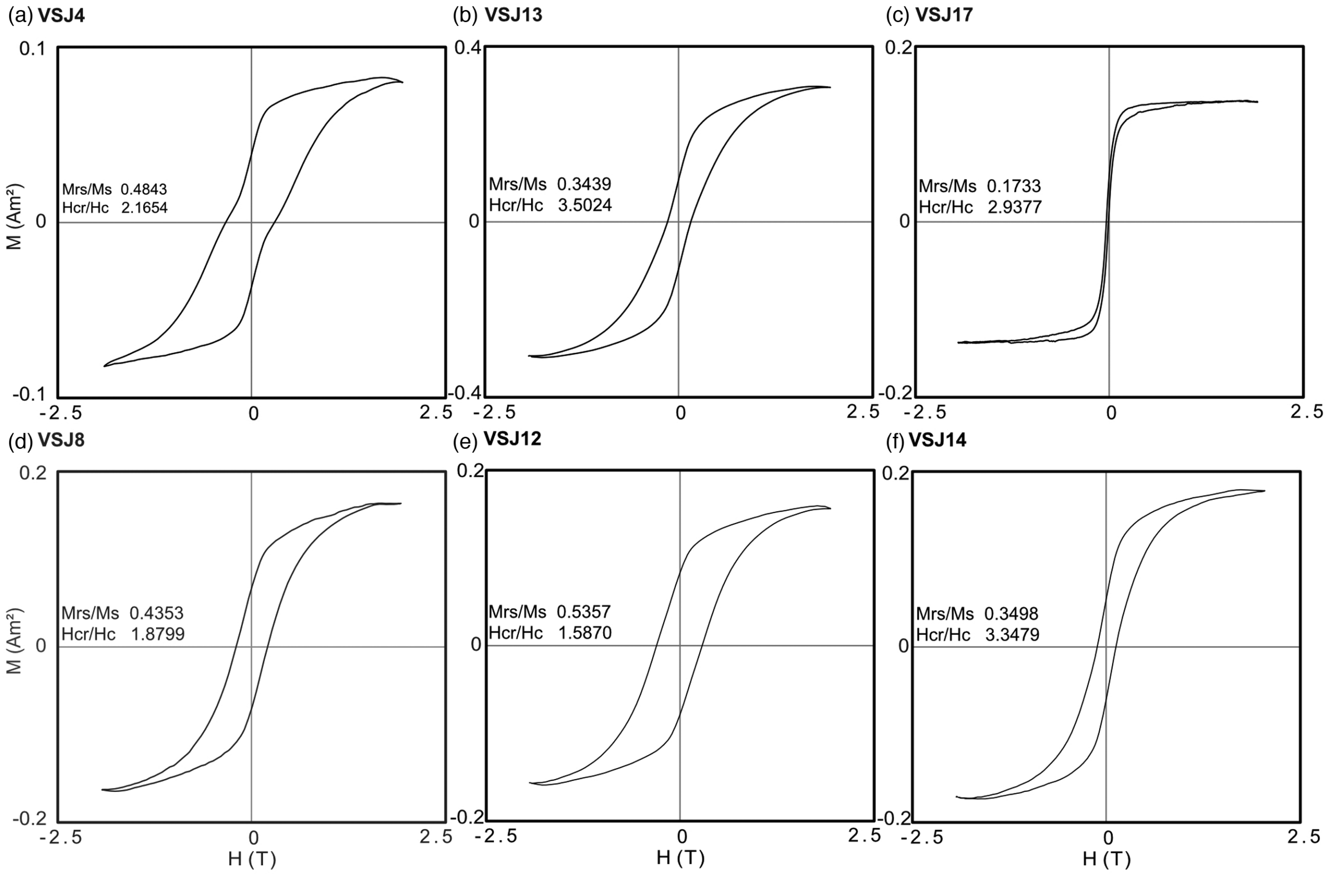

Figure 9. Representative hysteresis loops showing characteristic parameters ratios, saturation remanence (Mrs), saturation magnetization (Ms), and bulk coercive field (Hc). The loops are displayed after paramagnetic slope correction.

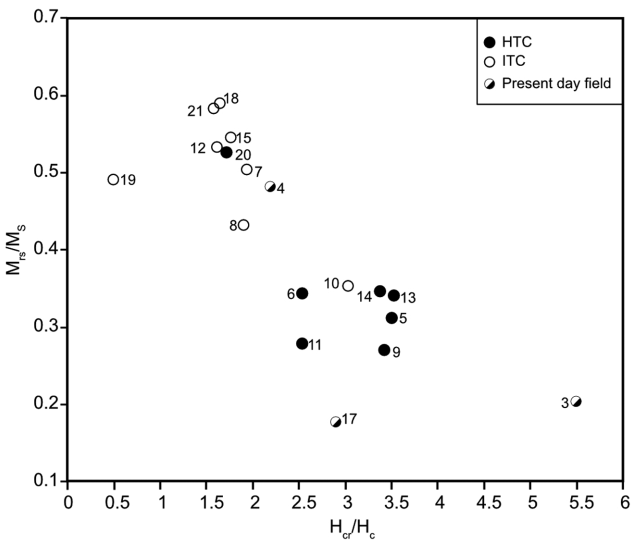

Figure 10. Modified Day plot (Day *et al.* 1977)) of the hysteresis ratios Mrs/Ms and Hcr/Hc for the samples of VSJ locality. The sites with a large recent component are indicated under 'Present-day field'. Samples with a larger HTC are indicated in closed circles, while samples with a larger ITC component are shown in open circles.

the total IRM. We thus conclude the following: goethite is not common and is generally absent; both the HTC and ITC observed in demagnetization of the NRM can be associated with IRM components of Hc > 150 mT consistent with their high resistance to AF demagnetization, the HTC, and the ITC thus reside in haematite; magnetite in small proportions is present in most samples.

Petrographic observations

Examples of the texture, shape, and size of the magnetic minerals carrying the magnetization in sandstones of the Zicapa Formation are shown in the SEM images (Fig. 13). Titanomagnetite pseudomorphs with exsolution textures replaced by haematite (Figs 13a and b), and with haematite substituting trellis texture (Fig. 13c) with sizes from 50 to 75 μm were found in most samples (examples shown are for VSJ4a and VSJ12). The trellis texture can be indicative of martite from former Ti-poor magnetite grains. Authigenic 'flakes' of haematite as cement with a size <5 μm are found in most of the samples (Fig. 13d).

Detrital grains and cement with cross-cutting relations are shown in the SEM backscattered images and in the reflected light images of the sandstones in the VSJ locality (Figs 13 and 14). Under transmitted light, at least three cement generations were observed. One primary cement was found in all samples, anisotropic red-coloured, and coating the framework grains. It was attributed to haematite; a secondary cement cuts across the primary clasts and cement, filling microfractures and it is constituted by calcite. The third type of cement is made of quartz and is found in the inter-pore space of the coarser sandstones as secondary after haematite. Detrital grains of martite with trellis texture (Figs 13c and 14a) were identified as a persistent and abundant phase in the samples. Laterite grains were observed as a lithic component in sandstones

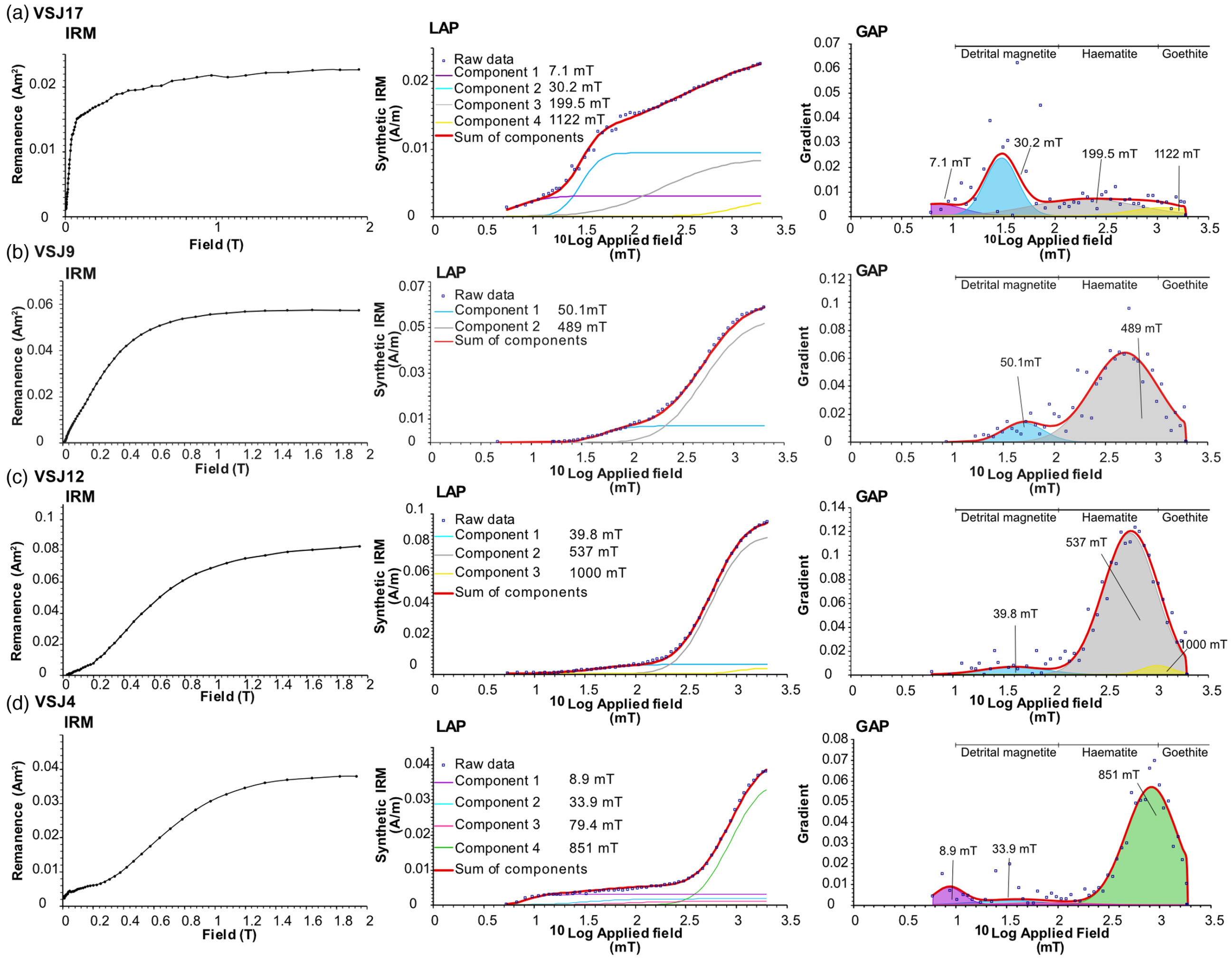

Figure 11. Representative samples of the IRM component analysis (Kruiver *et al.* 2001). From left to right the isothermal remanent magnetization plot (IRM), the linear acquisition plot (LAP) and the gradient acquisition plot (GAP) after Kruiver *et al.* (2001). In the LAP and GAP plots, open squares represent raw data points. The different components obtained are marked with different line colour (LAP) and fill colours (GAP). In the GAP the components with the major contribution to the magnetization are shown. IRM is in Am^2 kg^{-1}, log10 (H1/2) and DP are in log10 mT. Values of H1/2 are displayed with the colour code in the LAP. Identification of components in GAP after Abrajevitch *et al.* (2009) and reference therein.

ca. 10–20 mm (Fig. 14d) and were also observed as pebbles in conglomerates. Fig 13(c) shows textures of haematite grains with rutile inclusions. Haematite cement is also observed in pore spaces with euhedral habits, which indicate an authigenic origin. Euhedral haematite flakes occur in pore spaces perpendicular to detrital grain boundaries. Finally, branching textures of secondary haematite of relatively large grain-size were also found (Fig. 14f).

DISCUSSION

Magnetic carriers

Redbeds may include different magnetic minerals with different grain sizes ranging from MD to SD, resulting in contrasting coercivities and demagnetization behaviour. Defining the magnetic carriers is thus crucial for the interpretation of the results in terms of early or late acquisition of the magnetization, inclination shallowing correction, and/or remagnetization.

The NRM of samples of the Zicapa Formation at the VSJ locality is multicomponent. The decrease in NRM intensity during thermal demagnetization between approximately 250 and 500 °C is generally attributed to fine-grained pigmentary haematite, and a narrow unblocking temperature distribution attributed to detrital haematite (Kodama 2012). We observed mainly univectorial behaviour in samples such as VSJ8B1, VSJ9A2, and VSJ13B above 200 °C (Fig. 3). These samples show unblocking of the remanence between 350 and 600 °C, and a narrow range of unblocking-temperatures at temperatures over 650 °C (Figs 3 and 4). This suggests that the magnetization may be carried by both detrital and pigmentary haematite; in these samples both haematite forms record a field direction of the same polarity. It is evident, however, that the proportion of the remanence residing in detrital or pigmentary haematite varies along the section, and may even vary within a single bed. In other cases, the component that may be attributed to detrital haematite carries a nearly antipodal magnetization to that of the pigmentary haematite (e.g. VSJ12 and VSJ14; Fig. 4).

The thermomagnetic curves show either a single magnetic phase with a Curie/Neel temperature of approximately 650 °C (Fig. 8a), a dominant magnetic phase with a Curie temperature of approximately 580 °C (Figs 8b and c), or inflections that suggest similar contributions to the magnetization form these two phases (Figs 8d–f). Because of the larger saturation magnetization of magnetite relative to haematite, the haematite signal is overwhelmed and hardly recognizable in samples such as Figs 8(b) and (c). Also, the Neel

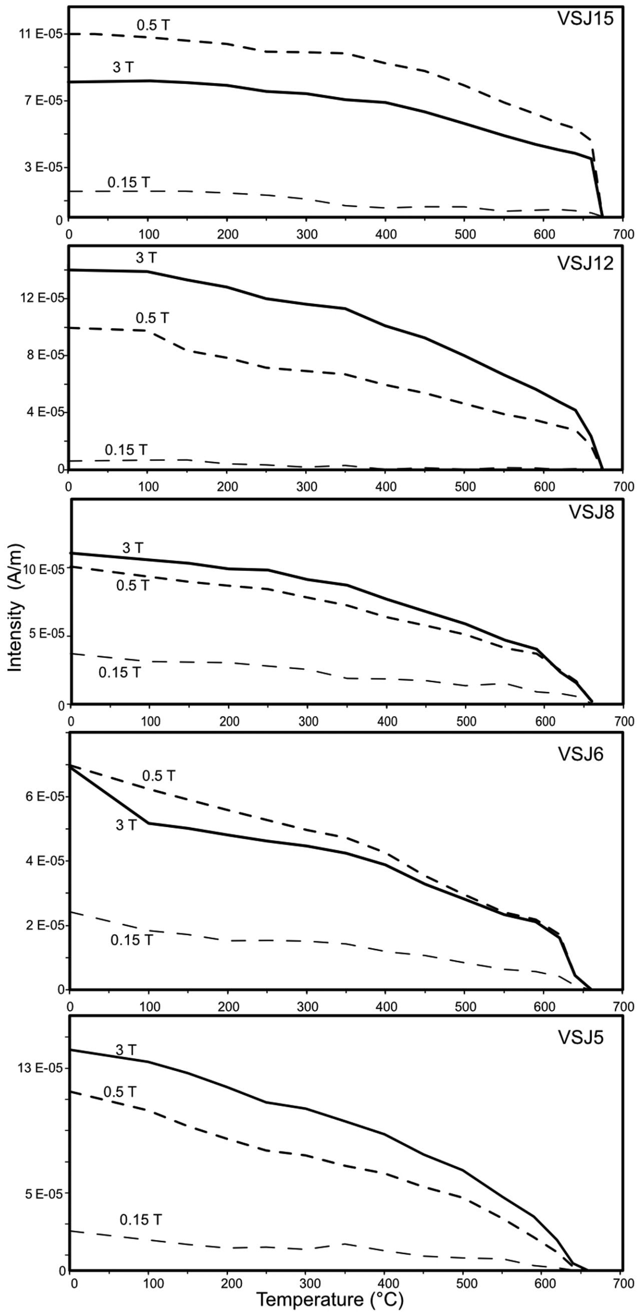

Figure 12. Thermal demagnetization of three orthogonal IRM components (Lowrie test). The hard and intermediate components reside in haematite, except in VSJ6 where there is a small contribution from goethite. The soft component (<150 mT) resides partly in magnetite and partly of low coercivity haematite.

temperature of haematite in samples such as Figs 8(d) and (e) are calculated at approximately 620 °C. Although this could be attributed to poor calibration of the thermocouple in the balance system, lower Neel temperatures have been observed when there is Al or Ti substitution in the haematite structure; this is our preferred interpretation. Thermomagnetic curves indicate the presence of low Ti-magnetite with a Curie temperature of approximately 570 °C, and haematite with a Neel temperature of 620 to 650 °C. On the other hand, the shape of the hysteresis loops and modelling of the IRM acquisition curves show that the magnetization in the VSJ locality cannot be solved by a single ferromagnetic phase. Rather, a mixture of particles with different coercivities is necessary to fit IRM curves and explain hysterresis loops.

Magnetic hysteresis properties and IRM curves

Rock magnetism results indicate that several magnetic phases are present in the red sandstones of the Zicapa Formations. Hysteresis loops indicate mixtures of different magnetic minerals, or particles with different grain-size, and thus coercivity. Thermomagnetic curves indicate the presence of nearly pure magnetite as well as haematite. The natural remanence is multivectorial, with three magnetization components. Unmixing the signal from different magnetic phases recognized in the rock magnetic experiments, and assigning each component to a particular magnetization component is a challenge. We attribute the LT component to MD magnetite, or occasionally goethite. The ITC and HTC reside in haematite.

From modelling of IRM acquisition curves (Fig. 11) we can identify at least two different components in terms of coercivities, but more commonly three or four components are necessary to get acceptable fits in the model (Kruiver *et al*. 2001). The dominant component is characterized by coercivities ($H_{1/2}$) between 400 and 600 mT, with somewhat narrow distributions (Figs 11b and c). This component of the IRM is likely to represent haematite particles that record the intermediate and the high unblocking temperature components of the NRM.

The weakest representative component in the IRM curves (generally contributing about 5 per cent to the total IRM) has an $H_{1/2}$ between 5 and 10 mT and is found in most samples in a small proportion. The weight in the IRM of this component relates to samples that carry a relatively large north-directed recent component (e.g. Fig 3b), supporting the viscous origin of this NRM component. Usually, the peak for this component is wide, which can be interpreted as a wide distribution of MD particles of low Ti-magnetite (according to thermomagnetic curves) of detrital origin (Fig. 13f). The maximum induction used in the IRM acquisition may be insufficient to fully detect goethite in the models. Although Lowrie tests show that goethite is not common, it may carry an LT component in some sites.

Samples such as VSJ4 illustrate an LT component as dominant in the NRM. This sample exhibits a remanence made of two components: a very low-unblocking-temperature recent magnetization in the direction of the modern geomagnetic field, and the intermediate magnetization of distributed unblocking temperature (Fig. 3b). The north-directed component is prominent (62 per cent of the NRM intensity; Table 3), and there is only very small or nearly insignificant component with high unblocking temperature. The sharp drop of the NRM intensity at <100 °C (Fig. 3b) may reside in a hard phase such as goethite. A Lowrie test is not available for this site to confirm this and no clear indication of goethite was observed in thermomagnetic curves, but at site VSJ6 with similar demagnetization behaviour we recognized goethite in the Lowrie test. MD magnetite also contributes significantly to this NRM component in VSJ4 because the north directed overprint is only completely removed upon heating to 200 °C. The presence of MD magnetite in VSJ4 is supported by IRM modelling and thermomagnetic curves (Fig. 11d). This sample is also characterized by a square hysteresis loop with very high coercivity (Fig. 9a). The magnetization of distributed unblocking temperatures is carried, most likely, by high coercivity authigenic haematite.

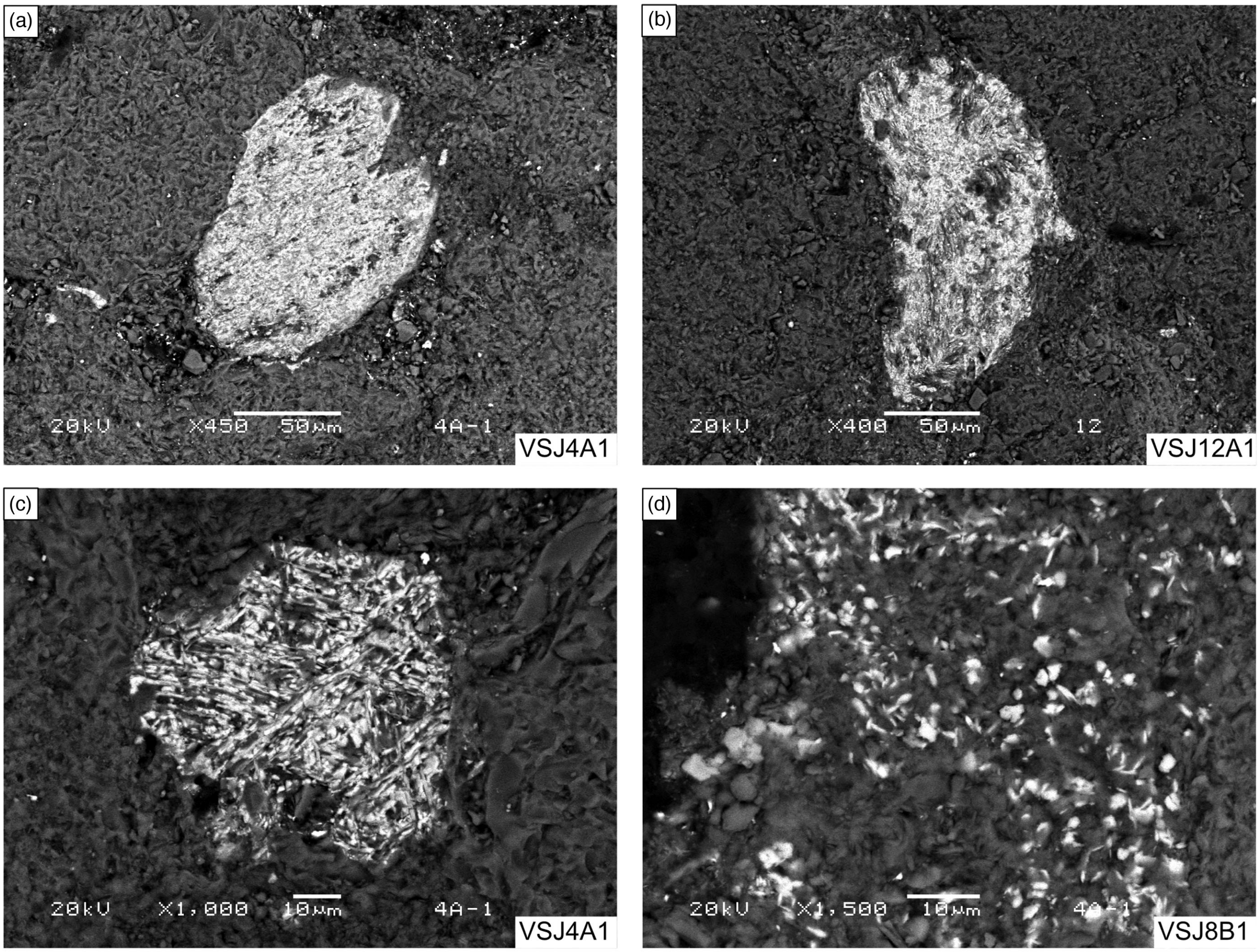

Figure 13. SEM back-scattered electron image of sandstone samples from the VSJ locality. (a and b) Large specularite grains. (c) Magnetite pseudo-morph complete altered to haematite. The haematite grows in three different directions (martite). (d) Secondary pigmentary haematite as cement in the sandstones from VSJ4.

Samples such as VSJ17, from a site where no stable remanence was observed, lack the IRM component with $H_{1/2}$ of 400–600 mT commonly observed at other sites (Table 3; Figs 4d and 11a). Instead, the dominant IRM signal is from a phase with a coercivity similar to that reported for MD magnetite (Abrajevitch *et al*. 2009). This example, for which the IRM is solved with four components, 80 per cent of the total contribution is from particles with $H_{1/2} < 200$ mT. This sample is also characterized by a narrow hysteresis loop (Fig. 9c), and a thermomagnetic curve with only one clear inflection point around 580 °C (Fig. 8c). According to the magnetic properties of the sample, the main carrier of the magnetization is interpreted as low Ti-magnetite. This sample carries a relatively large north-directed magnetization with a maximum unblocking temperature of *ca.* 200 °C and maximum coercivities of 20 mT (as seen in the AF pilot tests) but carries no stable magnetization residing in haematite (Fig 4d).

All the observations thus point to the nearly ubiquitous presence of a soft magnetic phase with the lowest coercivity, which is the most likely carrier of a viscous remanence. This component of the IRM will not be considered further, as demagnetization experiments suggest that the viscous component it carries is completely removed by heating to approximately 200 °C (Figs 3 and 4). The Lowrie tests also indicate that a magnetization in the direction of the recent dipole field resides in magnetite, and that one residing in goethite is observed only at very few sites.

For sample VSJ9, the modelled IRM shows a total contribution to the IRM of 94 per cent for particles with $H_{1/2}$ *ca.* 500 mT, with one component (6 per cent contribution) of $H_{1/2}$ of *ca.* 50 mT (Fig. 11b). The LTC component in this site is insignificant (Fig. 3d). The component with coercivities around 500 mT is characterized by an ample peak in the GAP diagram, which indicates that the corresponding population of ferromagnetic grains has a wide coercivity range as a response to a distribution grain-size and/or composition (Abrajevitch *et al*. 2009). This sample is characterized by a relatively large magnetization component residing in particles with unblocking temperatures >650 °C (Fig. 3); this magnetization of high unblocking temperature and high resistance to AF demagnetization is likely carried by specular or detrital haematite with an IRM signal of high $H_{1/2}$, but not greater than about 500 mT (Table 3).

Laboratory unblocking temperatures (Figs 3 and 4) and thermomagnetic curves (Fig. 8) suggest that the remanence resides primarily in the fine-grained haematite fraction, which is consistent with Collinson (1974) who attributes this behaviour to pigmentary haematite. In most of the samples less than 30 per cent of the remanence remains after heating to 600 °C, but with some exceptions

Table 3. Summary of the palaeomagnetism and rock magnetism results for the VSJ locality. The results are in stratigraphic order, and the main lithology for each site is indicated.

			NRM relative intensity			Magnetic properties						
Site	Depht (m)	Lithology	LTC (%)	ITC (%)	HTC (%)	*T* Curie (° C)	Hc (mT)	IRM components (mT)				
VSJ18A1	0	Very fine-grained sandstone	16.7	53.3	30.0	540, 640	178.6636					
VSJ17A1	10	Coarse-grained sandstone				580	12.8782	7.1	30.2	199.5		1122
VSJ20C1	60	Medium-grained lithic sandstone	30.8	15.4	53.8	580, 620	213.2925					
VSJ19B2	65	very fine-grained sandstone	8.3	47.3	44.5	670	194.3647					
VSJ21A1	85	Very fine-grained sandstone	39.6	47.2	13.2	No data	146.3372					
VSJ15A2	90	Medium-grained lithic sandstone	19.7	54.4	26.0	580, 640	177.8711	10	70		446	
VSJ14A1	100	Medium-grained lithic sandstone	20.1	39.4	40.5	560, 640	92.60009	25	100		446.7	1000
VSJ13B1	105	Fine-grained sandstone	25.8	35.9	38.4	560, 640	104.5236	17.8	100		660.7	
VSJ12A1	110	Fine-grained sandstone	12.8	46.1	41.1	560, 640	165.3917		39.8		537	1000
VSJ11E1	125	Coarse-grained sandstone	28.5	26.3	45.3	540, 620	175.8687					
VSJ10C1	130	Medium-grained lithic sandstone	25.9	63.0	11.1	No data	87.89395	5.6	50.1	190.5	501.2	
VSJ9A2	140	Very fine-grained sandstone	11.6	25.6	62.8	No data	90.84353		50.1		489	
VSJ8B1	145	Very fine-grained sandstone	7.9	77.3	14.9	580, 620	141.8717					
VSJ7C1	150	Very, red to purple	12.2	70.7	17.1	540, 620	162.8903					
VSJ6A2	160	Medium-grained lithic sandstone	23.8	36.6	39.7	No data	129.4849		31.6		631	
VSJ5B1	168	Very fine-grained sandstone	20.2	37.1	42.7	540, 620	89.81049		31.6	251		
VSJ4C1	178	Fine-grained sandstone	62.2	21.1	16.8	640	236.4715	8.9	33.9	79.4	851	
VSJ3A1	182	Medium-grained lithic sandstone	37.7	32.9	29.5	580, 630	38.09765		31.6	251.2	631	1258

(Figs 3 and 4; Table 3). The fraction remaining after heating to 600 °C represents a maximum of approximately 63 per cent of the remanence in samples such as VSJ9 (Figs 3d, Table 3); this fraction is very small in samples such as VSJ4 and VSJ8 (Figs 3b and c, Table 3). This fraction of the NRM is attributed to detrital (specular haematite).

As mentioned above, IRM acquisition curves were modelled components with coercivity components around 500 mT. We note, however, that some samples suggest that slightly higher coercivities ($H_{1/2} > \sim 600$ mT) are required to model the curves for the samples where the HTC is large or dominant. For instance, lower coercivities ($H_{1/2} < \sim 500$ mT) are required to model IRM curves for samples VSJ14 and VSJ15 where the distributed unblocking temperature component of the NRM (ITC) is more important (Table 3). This observation is tentative because throughout the study we observed, as has been pointed out before, that different techniques (hysteresis, IRM, and median destructive fields of AF demagnetization) result in different estimates of coercivity. It is thus difficult to show a consistent correspondence between coercivities of the ITC and the HT component, but there is a hint of higher coercivity for specular haematite. Hysteresis, however, appears to discriminate between a dominant authigenic component and a dominant detrital component.

There is a good correlation between hysteresis ratios and the nature of the remanence carriers inferred from demagnetization behaviour (Fig. 10). Higher Hcr/Hc ratios (between *ca.* 2.5 and 3.7) and lower Mrs/Ms ratios (between *ca.* 0.28 and 0.35) are observed for samples where the high-temperature remanence component is significant: making more than approximately 40 to 63 per cent of the NRM (Table 3). Lower Hcr/Hc ratios (between *ca.* 1.5 and 2) and higher Mrs/Ms ratios (between *ca.* 0.43 and 0.58) are observed for samples where the high-temperature remanence is small: making less than approximately 15 per cent of the NRM. This correlation breaks down when there is a large viscous remanence or where there is evidence of goethite, which probably indicates that the magnetite affects the hysteresis ratios, as is evident by the anomalous position of samples 3 and 17 in Fig. 10. The Hcr/Hc and Mrs/Ms ratios of the group of samples where the remanence is dominated by the component of distributed unblocking temperature (ITC) are consistent with ratios reported by Özdemir & Dunlop (2014) for SD haematite grains, perhaps suggesting that internal strain induced coercivity or crystal lattice defects may be reduced in the large (>10 μm) SD particles of detrital origin such as laterite fragments.

Particle grain size

Mixtures of different mineral grain-sizes are evident in the rock magnetic experiments (thermomagnetic curves, hysteresis loops and IRM acquisition curves), and the microscope observations indicate the presence of (generally) >10 μm detrital particles and <1 μm authigenic particles. The presence of components with different coercivities is well supported by hysteresis loops and IRM acquisition curves (Figs 9 and 11).

Laboratory determined median particle sizes of the single domain (SD) haematite range from 0.1 to 0.6 μm (Dunlop & Özdemir 2002), but SD behaviour is observed over a wide range of grain-sizes up to tens of μm. MD behaviour is observed in larger particles in the grain size range from ∼200 to 5 mm (Özdemir & Dunlop 2006). Values of magnetization saturation from the hysteresis experiments in both SD and MD particles show a great variation in the values from 270 Am^2 kg^{-1} in SD particles and near 9 $Am^2 Kg^{-1}$ in MD particles (Özdemir & Dunlop 2014). From SEM and petrographic observations, the particle size in the VSJ samples ranges from 10 to 300 μm in the detrital haematite (martite, specularite) and from approximately 0.2 to 1 μm in the pigmentary haematite flakes (Figs 13 and 14). We also determined values of magnetization saturation from 80 to 306 Am^2 kg^{-1} and Hc values from 131 to 350 mT. Our data have Hc and Mrs values comparable with those obtained for the fraction between 0.1 μm and 2 mm by other authors (e.g. Dankers 1981; Bao *et al*. 2011; Özdemir & Dunlop 2014). We thus consider that despite having large grains of haematite in the detrital fraction, the main contribution to the bulk magnetization is given by the small fraction (pigmentary haematite), which are single domain particles of relatively low laboratory unblocking temperature.

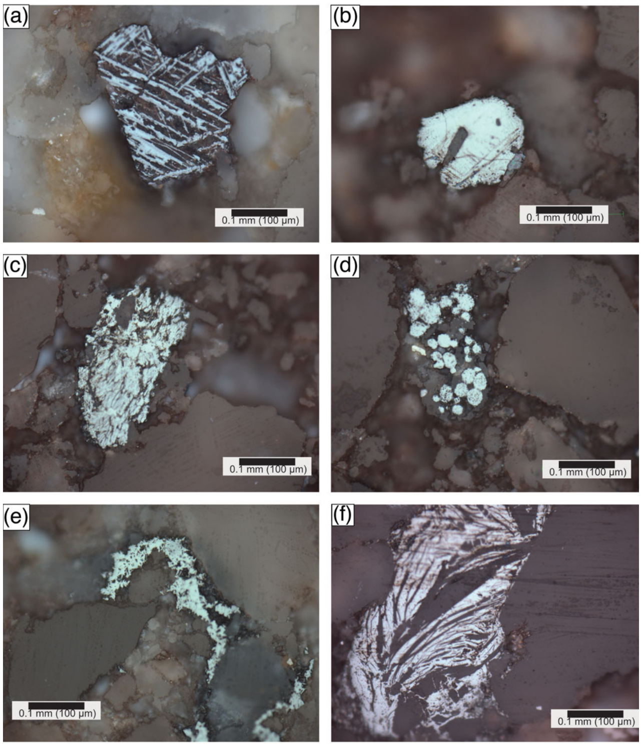

Figure 14. Petrographic characteristics of some magnetic carriers under reflected light. (a) Sample VSJ4, *in situ* alterations of ilmenite grain to leucoxene (rutile and anatase) in a trellis texture. (b) Sample VSJ12, anisotropic specularite grain with internal reflections. (c) Sample VSJ12, detrital haematite (specularite grain). (d) Sample VSJ12, oolithic haematite in a laterite grains. (e) Sample VSJ8, pigmentary haematite as a coating of quartz grains. (f) Sample VSJ4, haematite in lamellas as a product of alteration of a larger grain.

Magnetostratigraphy

The high temperature (600 to >650 °C) component or characteristic remanent magnetization of the sites in the VSJ locality was used to determine the polarity at the time of deposition, and with this, we propose a magnetic polarity zonation consisting of eight magnetozones defined on the basis of VGP latitudes. At sites VSJ8 and VSJ10, the polarity of the HTC is reverse in two samples, with a normal polarity in the rest. We assume that samples in the lower part of each bed record a reverse polarity. The reversal sequence can be correlated with the M10n to M3r chrons, from 132 to 129 Ma in the geomagnetic polarity time scale (Ogg 2012; Fig 2). The correlation is supported by geochronological constraints, with maximum depositional ages between *ca.* 149 ± 1 Ma (for the underlying San Juan de la Joya Member) and 133 ± 3 Ma for the overlying San Andrés Member (Sierra-Rojas & Molina-Garza 2014). Available palaeontological data of the overlying Morelos Formation also constraint the age of deposition of the Zicapa Formation as pre-Albian (Hernández-Romano *et al*. 1997).

Climate

Redbeds have been related to climatic conditions over the geologic time (Walker 1967a; Walker 1967b; Van Houten 1973; Besly & Turner 1983), indicating prolonged arid climatic conditions or strong seasonality. Sedimentological and depositional environment observations in continental redbeds show that alternations between wet and dry seasons in a monsoonal climate can favour the formation of redbeds (Dubiel & Smoot 1994; Parrish *et al*. 1998). On the other hand, early diagenesis has been proposed to be the origin of the haematite carrying the magnetization in redbeds in continental (as well as shallow marine) environments, locking the remanence in periods of $<10^2$ ka after deposition (Whidden *et al*. 1998). Also, hydrological conditions in palaeosols have been suggested as the mechanism responsible for the precipitation of haematite, and not a long seasonal or climatic condition (Sheldon 2005); but this also translates into the acquisition of an early chemical magnetization after the deposition.

Evidence of an arid and monsoonal climate during the Early Cretaceous is found in the continental deposits in southern Mexico (Sierra-Rojas *et al*. 2016), where anabranching river systems were formed under arid conditions allowing the generation of calcareous concretions in palaeosols. The Early Cretaceous climatic conditions in southern Mexico have also been considered arid because of the deposition of evaporitic units (e.g. Huitzuco Anhydrite) and the association of limestones and gypsum in the Guerrero Morelos platform (Gonzalez-Pacheco 1991; Hernández-Romano *et al*. 1997; Sierra-Rojas & Molina-Garza 2014).

In the San Juan de la Joyas locality, the presence of laterite pebbles is common in conglomerates. We show the presence of laterite grains in the sandstones of the VSJ locality, consisting of oolite of 5– 20 μm (Fig. 14d). Reflected light petrography shows as well the presence of goethite that may indicate the association haematite-goethite found in oolithic laterites in nickeliferous ores (Katzagiannakis *et al*. 2014), in ferruginous concretions in shallow marine sediments (Nejbert & Jurewicz 2004), in ferruginous oolithic laterites in tropical environment, and oolithic haematite-bearing ironstones (Hodych *et al*. 1985). Rather than indicating an Early Cretaceous tropical environment, the laterite grains observed in the Zicapa Formation were probably derived from Jurassic flood-plain deposits of the Tecocoyunca Group and later transported to the fluvial systems of the Zicapa basin.

CRM as early diagenetic process

As we demonstrated above, the sediments in the VSJ locality acquired both CRM and DRM which are represented by ITC and HTC respectively. The fact that the chemical magnetization was affected by burial compaction as demonstrated by the inclination shallowing in the site means indicate that the chemical magnetization, despite being secondary in origin, must have been acquired soon after deposition. Previous work has shown that acquisition of chemical magnetization can occur even before compaction (Liebes & Shive 1982; Tan *et al*. 2007; Kodama 2012 and references therein).

The sedimentological trends of the Ajuatetla Member of the Zicapa Formation suggest continuous deposition, without evident erosional contacts or long-lasting periods of no deposition. Based on the magnetostratigraphy and the geochronological constraints, we estimate for the Ajuatetla Member an undecompacted sedimentation rate of ∼36 m my^{-1}, which is comparable with the average sedimentation rates calculated for intra-arc extensional basins of 43 m my^{-1} (Stern 2010) and for near-shore marine deposits of 100–1000 m my^{-1} (Kodama 2012).

The magnetization component with high narrow unblocking-temperatures in the >600 °C temperature range is interpreted to be carried by detrital haematite. In intervals that contain polarity transitions (e.g. VSJ14 to VSJ15, Figs 2 and 5) in the sites with clear multicomponent behaviour (e.g. VSJ14), while the high-temperature component or ChRM records a DRM like the underlying site (VSJ13), the intermediate temperature components (350–500 °C) records the polarity of the site above it (VSJ15). This component is usually attributed to pigmentary haematite. It thus seems that while a sediment acquired a DRM at the time that it was deposited, the underlying layer is already acquiring a CRM.

At the VSJ locality the acquisition of a delayed CRM occurs not only at the transition R-N polarity between sites VSJ14 and VSJ15, it is also observed in sites below VSJ14 such as VSJ12 and VSJ13 about 12 and 10 m below the transition, respectively (Fig. 2). In site VSJ10 although the record is complex, the ITC is of reverse polarity and the HTC is normal in two specimens. A delayed CRM of opposite polarity to the HTC is observed at seven stratigraphic levels, with the ITC generally recording a normal polarity magnetization. Both the high and intermediate temperature magnetizations record normal and reverse polarities, indicating the prevalence of the phenomenon of early magnetization in pigmentary haematite in the Zicapa red beds. We consider a continuous minimum undecompacted sedimentation at a rate of ∼35 m my^{-1}, calculated from the magnetostratigraphic correlation. Using this value we can roughly estimate a maximum time of precipitation of the pigmentary haematite carrying the ITC. For instance, site VSJ12 records the ITC about 300 kyr (12 m) after deposition.

Yet another way to approximate the time of CRM acquisition is by the thickness of the interval of strata of opposite polarity to that of the DRM, but similar to the CRM. For instance, approximately 7 m of strata of normal polarity and 15 of reverse polarity overlie site VSJ14, where the DRM is reverse but the CRM is normal. For a sedimentation rate of 35 m my^{-1}, this suggests that the CRM is locked-in less than about 200 kyr after deposition. These results are congruent with estimates previously presented in literature, in similar depositional and climatic environments as the ones at the time of deposition of the Zicapa Formation (Whidden *et al*. 1998).

Tectonic implications

The tilt corrected directions show nearly the same dispersion as in-situ directions because the entire locality was sampled in a single anticline limb and dip directions vary only slightly (Fig. 1). However, the mean direction obtained before *E*/*I* correction in the VSJ locality (Dec = 272.5°, Inc = 16.5°) does not resemble the Early Cretaceous to Cenozoic expected direction for the North America craton (McElhinny & McFadden 2000), nor the directions observed in Upper Cretaceous strata (Dec = 323.1, Inc = 36.5; Molina-Garza *et al*. 2003) or Cenozoic strata (Dec = 340.8°, Inc = 34.3°; Molina-Garza & Ortega-Rivera 2006) in the Guerrero-Morelos platform in nearby sites. This suggests that a regional remagnetization has not affected Zicapa strata, as it appears to have affected shallow marine limestones of the Morelos Formation (Molina-Garza *et al*. 2003). Furthermore, the record of both polarities suggests that the magnetization is of primary, or near primary origin. The HTC is interpreted as the ChRM of the Zicapa Formation redbeds. We argue that both the intermediate and high-temperature components predate compressional Laramide age (latest Cretaceous) deformation of the Sierra Madre del Sur. The age of the magnetization can be constrained by the maximum depositional age of the Zicapa Formation of Hauterivian-Barremian age (Sierra-Rojas & Molina-Garza 2014), and correlation with the geomagnetic polarity time scale (Fig. 2).

The ChRM is rotated counter-clockwise with respect to the North American reference direction (Torsvik *et al*. 2012). Both the ITC and the HTC indicate a counter-clockwise rotation of approximately 60°; latitudinal displacement is uncertain, however. The ITC inclination indicates statistically significant inclination anomaly ($F = -16.8 \pm 12.7$), but there is not flattening ($F = -7.7 \pm 13.0$) for the HTC. Because of the possibility of unremoved overprints in the ITC, we lend more credibility to the flattening estimate of the HTC. It is unclear if the rotation is a regional or a local phenomenon, but we tend to support rotation about a local vertical axis. Counter-clockwise rotation about a local vertical axis has been previously reported for localities in the Guerrero-Morelos platform (Molina Garza *et al*. 2003), and it is thought to be related to strike-slip tectonics along the southwest Mexican margin.

CONCLUSIONS

Samples from the Ajuejutla Member of the Zicapa Formation have a multivectorial NRM. Widespread, there is a north-directed magnetization of low unblocking temperature (<200 °C). Rock magnetic experiments suggest that this is carried by a magnetic phase with a Curie temperature near 580 °C, and IRM curves suggest has coercivities ∼10 mT. It is interpreted as a viscous component, for which rock magnetism and petrography strongly suggest the carrier is MD detrital magnetite. In general, however, the NRM is mostly dominated by an intermediate laboratory unblocking temperature component. This component shows distributed laboratory unblocking-temperatures between *ca.* 300–500 °C. An additional component is of high, discrete, laboratory unblocking-temperatures (600 to >650 °C). Curie–Neel temperatures ∼620 to 670 °C, and relatively high coercivity (>∼450–650 mT) indicate that the principal remanence carrier of the intermediate and high-temperature components is haematite. The ITC and HTC may be near parallel to each other or anti-parallel, which indicates that both polarities may be recorded in some samples. In some sites (beds) the intermediate unblocking temperature component is of both normal and reverse polarity, but the high temperature is of uniform polarity. Often, the polarity of the intermediate component corresponds to the polarity of the overlying strata.

The intermediate temperature component is interpreted as a CRM obtained early after deposition, and is carried by authigenic haematite. The high-temperature component is interpreted as a DRM. Magnetic carriers, inferred from observations in SEM as well as petrographic inspection of thin sections, are laterite grains and specularite with high-temperature textures (trellis texture).

Hysteresis parameters of the samples of the VSJ locality show evidence of a mixture of magnetic minerals with contrasting coercivities, or different grain size distributions (single-domain and multidomain). IRM acquisition curves require modelling with a minimum of two, but more often three or four components. Also, lower Hcr/Hc ratios (between *ca.* 1.5 and 2) and higher Mrs/Ms ratios (between *ca.* 0.43 and 0.58), comparable to those of SD haematite (Özdemir & Dunlop 2014), are observed for samples where the high-temperature remanence (DRM) is small and the remanence is interpreted as a CRM. Hcr/Hc ratios are higher (between 2.5 and 3.7) for samples with a substantial DRM (Fig. 10).

In the Zicapa Formation, a large fraction of the remanence resides in fine-grained authigenic SD haematite (Fig. 9). This suggests, in turn, that as little as 36 per cent (e.g. sample VSJ12) and as much as 77 per cent of the remanence (e.g. sample VSJ8) is of chemical origin. Authigenic haematite (<1 μm in size) was identified as fine-grained early cement in pore spaces with euhedral habits, euhedral haematite flakes occur in pore spaces perpendicular to detrital grain boundaries, and branching textures of secondary haematite of relatively large grain-size (>100 µm in size) were also found.

Early CRM in redbeds can be inferred from demagnetization behaviour, magnetostratigraphy, SEM observations, and rock magnetism. We emphasize the VSJ14 to VSJ15 transition of polarity, where an early acquisition of chemical magnetization was determined to be acquired in a maximum of approximately 0.5 Ma.

Even with an important amount of the magnetization residing in pigmentary haematite, corrections for inclination shallowing of the palaeomagnetic data were necessary according to elongation/inclination analysis. However, the fact that the inclination of chemical magnetization was affected by compaction, is considered as evidence of an early chemical magnetization. The overall means of the intermediate and high-temperature components are $D = 282.0$, $I = 12.4^{\circ}$, $k = 13.33$, $n = 17$ and $D = 272.5$, $I = 16.5^{\circ}$, $k = 14.04$, $n = 11$; after correction for inclination shallowing with an f factor of 0.41 and 0.4 the corresponding inclination are 28.2° and 36.5°, respectively. The ChRM is rotated counter-clockwise with respect to the North American reference direction approximately 60°.

ACKNOWLEDGEMENTS

We acknowledge the Programa de Apoyo a Proyectos de Investigación e Innovación Tecnológica (PAPIIT: IN104511–3) for funds to support the fieldwork. We also acknowledge partial support from CONACYT grant 129862 to RSMG. We thank Jorge Escalante for the technical assistance provided in the Laboratorio de Paleomagnetismo y Magnetismo de Rocas, Centro de Geociencias, UNAM, Juan Tomás Vázquez for preparation of thin sections and Dr Marina Vega for assistance with the SEM images.

REFERENCES

Abrajevitch, A., Van der Voo, R. & Rea, D.K., 2009. Variations in relative abundances of goethite and hematite in Bengal Fan sediments: Climatic vs diagenetic signals, *Mar. Geol.,* **267**(3–4), 191–206.

Bao, L., Yang, H., Wang, X., Zhang, F., Shi, R., Liu, B., Wang, L. & Zhao, H., 2011. Synthesis and size-dependent magnetic properties of single-crystalline hematite nanodiscs, *J. Cryst. Growth,* **328**(1), 62–69.

Beck, M.E., Jr., 1980. Paleomagnetic record of plate-margin tectonic processes along the western edge of North America, *J. geophys. Res.,* **85**(B12), 7115–7131.

Beck, M.E., Burmester, R.F. & Housen, B.A., 2003. The red bed controversy revisited: shape analysis of Colorado Plateau units suggests long magnetization times, *Tectonophysics,* **362**(1-4), 335–344.

Besly, B.M. & Turner, P., 1983. Origin of red beds in a moist tropical climate (Etruria Formation, Upper Carboniferous, UK), *Geol. Soc. London Spec. Publ.,* **11**(1), 131–147.

Butler, R.F., 1998. *Paleomagnetism: Magnetic Domains to Geologic Terranes,* Blackwell Scientific Publications, p. 319.

Cabral-Cano, E., Lang, H.R. & Harrison, C.G.A., 2000. Stratigraphic assessment of the Arcelia–Teloloapan area, southern Mexico: implications for southern Mexico's post-Neocomian tectonic evolution, *J. South Am. Earth Sci.,* **13**(4–5), 443–457.

Collinson, D.W., 1974. The role of pigment and specularite in the remanent magnetism of red sandstones, *Geophys. J. Int.,* **38**(2), 253–264.

Dankers, P.H.M, 1981. Relationship between median destructive field and remanent coercive forces for dispersed natural magnetite, titanomagnetite and hematite, *Geophys. J. Int.,* **64**(2), 447–461.

Day, R., Fuller, M.D. & Schmidt, V.A., 1977. Hysteresis properties of titanomagnetites: Grain size and composition dependence, *Phys. Earth Planet. Inter.,* **13**, 260–267.

Demarest, H.H., 1983. Error analysis for the determination of tectonic rotation from paleomagnetic data, *J. geophys. Res.,* **88**(B5), 4321–4328.

Dubiel, R.F. & Smoot, J.P., 1994. Criteria for interpreting paleoclimate from red beds-a tool for Pangean reconstructions, in *Pangea: Global Environment and Resources*, pp. 295–310, eds Embry, A.F., Beauchamp, B. & Glass, D.J., Canadian Society of Petroleum Geologist.

Dunlop, D.J., 1986. Hysteresis properties of magnetite and their dependence on particle size: a test of pseudo-single-domain remanence models, *J. geophys. Res.,* **91**(B9), 9569–9584.

Elston, D.P. & Purucker, M.E., 1979. Detrital magnetization in red beds of the Moenkopi formation (Triassic), Gray Mountain, Arizona, *J. geophys. Res.,* **84**(B4), 1653–1665.

Fisher, R.A., 1953. Dispersion on a sphere, *Proc. R. Soc. A,* **217,** 295–305.

Garcés, M., Parés, J.M. & Cabrera, L., 1996. Further evidence for inclination shallowing in red beds, *Geophys. Res. Lett.,* **23**(16), 2065–2068.

Gonzalez-Pacheco, V.V. 1991. *Evolución sedimentológica y diagénesis del Cretácico de la porción norte del Estado de Guerrero, MSc Thesis*, UNAM, México.

Hernández-Romano, U., Aguilera-Franco, N., Martínez-Medrano, M. & Barceló-Duarte, J., 1997. Guerrero-Morelos Platform drowning at the Cenomanian–Turonian boundary, Huitziltepec area, Guerrero State, southern Mexico, *Cretaceous Res.,* **18**(5), 661–686.

Hodych, J.P., Paetzold, R.R. & Buchan, K.L., 1985. Chemical remanent magnetization due to deep-burial diagenesis in oolitic hematite-bearing ironstones of Alabama, *Phys. Earth planet. Inter.,* **37**(4), 261–284.

Katzagiannakis, N., Alevizos, G., Stamboliadis, E., Stratakis, A. & Petrakis, E., 2014. Mineralogical investigation and washability treatment of the nickeliferous lateritic deposit of nome (Albania), *Geomaterials,* **4**(03), 105–115.

Kirschvink, L, 1980. The least-squares line and plane and the analysis of palaeomagnetic data, *Geophys. J. Int.,* **62**(3), 699–718.

Kodama, K.P. 2012. *Paleomagnetism of Sedimentary Rocks: Process and Interpretation,* John Wiley & Sons.

Kodama, K.P. & Dekkers, M.J. 2004. Magnetic anisotropy as an aid to identifying CRM and DRM in red sedimentary rocks, *Stud. Geophys. Geod.,* **48**(4), 747–766.

Kruiver, P.P., Dekkers, M.J. & Heslop, D., 2001. Quantification of magnetic coercivity components by the analysis of acquisition curves of isothermal remanent magnetisation, *Earth planet. Sci. Lett.,* **189**(3–4), 269–276.

Larson, E.E. & Walker, T.R., 1975. Development of chemical remanent magnetization during early stages of Red-Bed formation in Late Cenozoic Sediments, Baja California, *Bull. geol. Soc. Am.,* **86**(5), 639–650.

Larson, E.E., Walker, T.R., Patterson, P.E., Hoblitt, R.P. & Rosenbaum, J.G., 1982. Paleomagnetism of the Moenkopi Formation, Colorado Plateau: basis for long-term model of acquisition of chemical remanent magnetism in red beds, *J. geophys. Res.,* **87**(B2), 1081–1106.

Liebes, E. & Shive, P.N., 1982. Magnetization acquisition in two Mesozoic red sandstones, *Phys. Earth planet. Inter.,* **30**(4), 396–404.

Lowrie, W., 1990. Identification of ferromagnetic minerals in a rock by coercivity and unblocking temperature properties, *Geophys. Res. Lett.,* **17**(2), 159–162.

Maillol, J.M. & Evans, M.E., 1993. Permian palaeosecular variation as recorded in the Lodève redbeds, southern France, *Geol. Carpath*. **44,** 281–287.

Martini, M., Ferrari, L., López-Martínez, M. & Valencia, V.A., 2010. Stratigraphic redefinition of the Zihuatanejo area, southwestern Mexico, *Rev. Mex. Cienc. Geol.,* **27,** 412–430.

McElhinny, M.W. & McFadden, P.L., 2000. In *Paleomagnetism: continents and oceans*, Vol. 73, p. 1, eds Dmowska, R., Holton, J.R. & Rossby, H.T., Academic Press, San Diego.

McFadden, P.L. & McElhinny, M.W. 1990. Classification of the reversal test in palaeomagnetism, *Geophys. J. Int.,* **103**(3), 725–729.

Molina-Garza, R.S. & Ortega-Rivera, A., 2006. Chronostratigraphy and paleomagnetism of the Balsas Group in the Tuzantlán-Copalillo basin, northern Guerrero state, Mexico, *Rev. Mex. Cienc. Geol.,* **23**(2), 215–232.

Molina-Garza, R.S., Geissman, J.W. & Van der Voo, R., 1989. Paleomagnetism of the Dewey Lake Formation (Late Permian), northwest Texas:

end of the Kiaman superchron in North America, *J. geophys. Res.,* **94**(B12), 17 881–17 888.

Molina-Garza, R.S., Böhnel, H.N. & Hernández, T., 2003. Paleomagnetism of the Cretaceous Morelos and Mezcala formations, southern Mexico, *Tectonophysics,* **361**(3–4), 301–317.

Molina-Garza, R.S., Geissman, J.W., Van der Voo, R., Lucas, S.G. & Hayden, S.N., 1991. Paleomagnetism of the Moenkopi and Chinle Formations in central New Mexico: implications for the North American apparent polar wander path and Triassic magnetostratigraphy, *J. geophys. Res.,* **96**(B9), 14 239–14 262.

Nejbert, K. & Jurewicz, E., 2004. Mineralogy and petrography of the ferruginous concretions from siliciclastic Rhaetian deposit, Tatra Mountains, *Mineral. Soc. Poland-Spec. Pap.,* **24,** 299–302.

Ogg, J.G., 2012. Geomagnetic polarity time scale, in *The Geologic Time Scale 2012*, pp. 85–113, eds Gradstein, F.M., Ogg, J.G, Schmitz, M. & Ogg, G., Elsevier.

Özdemir, Ö. & Dunlop, D.J., 2002. Thermoremanence and stable memory of single-domain hematites, *Geophys. Res. Lett.,* **29**(18).

Özdemir, Ö. & Dunlop, D.J., 2006. Magnetic memory and coupling between spin-canted and defect magnetism in hematite, *J. geophys. Res.,* **111**(B12), doi:10.1029/2006JB004555.

Özdemir, Ö. & Dunlop, D.J., 2014. Hysteresis and coercivity of hematite, *J. geophys. Res.,* **119**(4), 2582–2594.

Parrish, J.T., Daniel, I.L., Kennedy, E.M. & Spicer, R.A., 1998. Paleoclimatic significance of mid-Cretaceous floras from the middle Clarence Valley, New Zealand, Palaios, **13**(2), 149–159.

Roberts, A.P., Cui, Y. & Verosub, K.L., 1995. Wasp-waisted hysteresis loops: mineral magnetic characteristics and discrimination of components in mixed magnetic systems, *J. geophys. Res.,* **100**(B9), 17 909–17 924.

Roy, J.L. & Park, J.K., 1972. Red beds: DRM or CRM?, *Earth Planet. Sci. Lett.,* **17**, 211

Sagnotti, L., Macrì, P., Egli, R. & Mondino, M., 2006. Magnetic properties of atmospheric particulate matter from automatic air sampler stations in Latium (Italy): toward a definition of magnetic fingerprints for natural and anthropogenic PM 10 sources, *J. geophys. Res.,* **111**(B12), doi:10.1029/2006JB004508.

Sheldon, N.D., 2005. Do red beds indicate paleoclimatic conditions?: a Permian case study, *Palaeogeogr. Palaeoclimatol. Palaeoecol.,* **228**(3–4), 305–319.

Sierra-Rojas, M.I. & Molina-Garza, R.S., 2014. La Formación Zicapa del sur de México: revisión estratigráfica, sedimentología y ambientes sedimentarios, *Rev. Mex. Cienc. Geol.,* **31**(2), 174–189.

Sierra-Rojas, M.I., Molina-Garza, R.S. & Lawton, T.F., 2016. The lower Cretaceous Atzompa Formation in South-Central Mexico: record of evolution from extensional backarc basin margin to carbonate platform, *J. Sediment Res.,* **86**(6), 712–733.

Steiner, M.B., 1983. Detrital remanent magnetization in hematite, *J. geophys. Res.,* **88**(B8), 6523–6539.

Stern, B., 2010, The anatomy and ontogeny of modern intra-oceanic arc systems, in *The Evolving Continents: Understanding Processes of Continental Growth*, pp. 7–34, eds Kusky, T.M., Zhai, M.G. & Xiao, W., Geological Society, London, Special Publications, 338, doi:10.1144/SP338.2.

Talavera-Mendoza, O., Ruiz, J., Gehrels, G.E., Valencia, V.A. & Centeno-García, E., 2007. Detrital zircon U/Pb geochronology of southern Guerrero and western Mixteca arc successions (southern Mexico): new insights for the tectonic evolution of southwestern North America during the late Mesozoic/, *Bull. geol. Soc. Am.,* **119,** 1052–1065.

Tan, X., Kodama, K.P., Gilder, S. & Courtillot, V. 2007. Rock magnetic evidence for inclination shallowing in the Passaic Formation red beds from the Newark basin and a systematic bias of the Late Triassic apparent polar wander path for North America, *Earth planet. Sci. Lett.,* **254**(3–4), 345–357.

Tauxe, L. & Kent, D.V., 1984. Properties of a detrital remanence carried by haematite from study of modern river deposits and laboratory redeposition experiments, *Geophys. J. Int.,* **76**(3), 543–561.

Tauxe, L. & Kent, D.V., 2004. A simplified statistical model for the geomagnetic field and the detection of shallow bias in paleomagnetic inclinations: was the ancient magnetic field dipolar?, in *Timescales of the Paleomagnetic Field*, pp. 101–115, eds Channell, J.E.T., Kent, D.V., Lowrie, W. & Meert, J.G., American Geophysical Union.

Tauxe, L., Kent, D.V. & Opdyke, N.D., 1980. Magnetic components contributing to the NRM of Middle Siwalik red beds, *Earth planet. Sci. Lett.,* **47**(2), 279–284.

Tauxe, L., Mullender, T.A.T. & Pick, T., 1996. Potbellies, wasp-waists, and superparamagnetism in magnetic hysteresis, *J. geophys. Res.,* **101**(B1), 571–583

Torsvik, T.H. *et al.*, 2012. Phanerozoic polar wander, palaeogeography and dynamics, *Earth Sci. Rev.,* **114**(3–4), 325–368.

Van der Voo, R. & Torsvik, T.H., 2012. The history of remagnetization of sedimentary rocks: deceptions, developments and discoveries, *Geol. Soc. London Spec. Publ.,* **371**(1), 23–53.

Van Houten, F.B., 1973. Origin of Red Beds a Review-1961–1972. *Annu. Rev. Earth Planet. Sci.*, **1**(1), 39–61.

Walker, T.R., 1967a. Formation of red beds in modern and ancient deserts, *Bull. geol. Soc. Am.,* **78**(3), 353–368.

Walker, T.R., 1967b. Color of recent sediments in tropical Mexico: a contribution to the origin of red beds, *Bull. geol. Soc. Am.,* **78**(7), 917–920.

Walker, T.R., Larson, E.E. & Hoblitt, R.P., 1981. Nature and origin of hematite in the Moenkopi Formation (Triassic), Colorado Plateau: a contribution to the origin of magnetism in red beds, *J. geophys. Res.,* **86**(B1), 317–333.

Whidden, K.J., Lund, S.P., Bottjer, D.J., Champion, D. & Howell, D.G., 1998. Paleomagnetic evidence that the central block of Salinia (California) is not a far-traveled terrane, *Tectonics,* **17**(3), 329–343.

Zijderveld, J.D.A., 1967. A.C. demagnetization of rocks: analysis of results, in *Methods in Paleomagnetism*, pp. 254–286, eds Collinson, D., Creer, K. & Runcorn, S., Elsevier Science B.V.